Using post-flood surveys and geomorphologic mapping to validate hydrological and hydraulic models: the flash flood of the Girona River (Spain) in 2007

Segura-Beltrán, F.[1]; Sanchis-Ibor, C.[2]; Morales-Hernández, M.[3]; González-Sanchis, M.[4]; Bussi, G.[5] and Ortiz, E[6].

1 Departament de Geografia, Universitat de València, Avda./ Blasco Ibáñez 28, 46010, València, Spain
2 Centro Valenciano de Estudios del Riego, Universitat Politècnica de València, 46022, València, Spain
3 Fluid Mechanics, LIFTEC-EINA, CSIC-Universidad Zaragoza, C/ María de Luna 3, 50018, Zaragoza, Spain
4 Department of Hydraulic Engineering and Environment, Universitat Politècnica de València, València, Spain
5 School of Geography and the Environment, University of Oxford, South Parks Road, OX1 3QY, Oxford, UK
6 Idrologia & Ambiente s.r.l. Via Stazio 66 80123 Napoli, Italy

Abstract

This paper analyses the River Girona (Spain) flash flood, occurred the 12th of October 2007, combining hydrological and hydraulic modeling with geomorphologic mapping and post-flood survey information. This research aims to reproduce the flood event in order to understand and decipher the flood processes and dynamics on a system of

overlapped prograding alluvial fans. The hydrological model TETIS was used to characterize the shape and dimension of the October 2007 River Girona hydrograph. Subsequently, the flood event was reproduced using the free surface flow module of the model RiverFlow2D. The combination of hydrological and hydraulic models was validated using post-flood surveys defining maximum flooded area and flood depths. Then, simulations with different peak discharges were carried out to estimate the hydro-geomorphologic response of the Girona River floodplain, through the identification of the activation thresholds in different geomorphic elements.

Results showed that the unit peak discharge of the October 2007 flood event was among the largest ever recorded in the area, according to the existing literature. Likewise, the hydraulic model showed a good performance (Fit_A = 76 %, RMSE = 0.65 m and NSE = 0.6), despite the complexity of the case, an ephemeral and ungauged river. The model simulation revealed the existence of a geo-chronological activation pattern of palaeochannels and alluvial fans, which was altered by the presence of a tectonic depression and bridges construction.

This multidisciplinary approach proved to be a useful strategy for understanding flash flood processes in ungauged catchments. It allowed understanding the mechanisms governing floods in alluvial fans systems and it represented a solid contribution for early warning plans and risk mitigation policies.

Keywords: Flash floods; hydrological modeling; hydraulic modeling; alluvial fans; post-flood surveys; geomorphologic mapping.

1. Introduction

Flash floods are a recurrent cause of damages and fatalities. According to Barredo (2007), 40% of the flood-related casualties occurred in Europe in the period 1950–2006 are due to this type of flood events, which take place in different geographical scenarios (Gaume et al., 2009; Marchi et al., 2010; Borga and Morin, 2014; Llasat et al., 2014). However, they are particularly frequent and relevant in ungauged ephemeral streams in arid and semiarid zones (House and Baker, 2001; Yatheendradas et al., 2008).These events are a consequence of intense rainfall and sudden runoff generation. The flash flood hydrographs have steep rising limbs, sharp peaks and large transmission losses (Nanson et al., 2002). The runoff coefficient has a high variability (Camarasa and Segura, 2001; Braud et. al., 2010) depending on basin lithology, soil characteristics and antecedent soil moisture.

In the Western Mediterranean region, flash floods usually occur in spring and autumn, when intense, heavy and irregularly distributed rain takes place (Segura, 1990; Camarasa and Segura, 2001; Barredo, 2007; Gaume et al. 2009). The particular conformation of the Mediterranean basin, with high mountain ranges close to the sea, steep slopes, sparse vegetation, thin soils and permeable rock, enhances the magnitude of these natural events. Alluvial fan coastal systems, such as the Girona River floodplain (eastern Spain), introduce a major complexity on flooding processes and risk management (Segura, 2003; Santangelo et al., 2012), because of the uncertainty derived from convex topography, channel mobility and overlapping sequences.

The impact of flash floods in this region is increased by the intense human use of the narrow Mediterranean coastal plains. These areas, densely populated, concentrate the most part of the urban developments, infrastructures and economic activity of the region. The absence of sound territorial planning in these vulnerable areas usually worsens the consequences of flash floods (Barrera et al., 2006; Lara et al., 2010; Camarasa-Belmonte and Soriano-García, 2012). For these reasons, improving the knowledge on these phenomena is a critical factor in developing resilient adaptation strategies (Creutin et al., 2013).

Despite the fact that there are numerous studies on flash floods, event comprehension and flood risk management are not easy tasks. In the last decade, numerous hydrological (Pilgrim et al., 1988; Vélez and Francés, 2005; Braud et al. 2010) and hydraulic models (Hall et al., 2005; Bates et al., 2006; Pappenberger et al., 2005 and 2007; Schuman et al. 2009; Di Baldassare et al. 2009; Murillo and García-Navarro, 2010; Lacasta et al., 2014) have been developed to simulate flood hydrographs and flooded areas. However, the specific space-time scales of flash flood events, the lack or scarcity of rainfall and stream flow data, and the short lag time are a cause of high uncertainty. In order to overcome these difficulties, flash flood modeling requires an integrated approach that includes, besides the hydrological and hydraulic models, information such as hydro-geomorphic mapping and post-flood surveys (Borga, et al. 2011; Gaume and Borga, 2008; Marchi et al. 2010) so as to incorporate qualitative information to achieve a better understanding of flood processes.

This study analyses the River Girona flash flood, occurred the 12th of October 2007. This event caused one casualty and material damages to 1.000 buildings, 1.500 vehicles and numerous infrastructures. Rainfall parameters were exceptional, in terms of intensity and accumulated precipitation. In some locations, more than 400 mm accumulated rainfall was registered in 48 hours. The fact that this flash-flood has been well documented (Segura, 2009; Pastor et al., 2010) and the development of geomorphologic works bring us some new approaches in order to test hydrological and hydraulic models, considering post-flood surveys and hydro-geomorphic mapping in order to validate the hydrologic and hydraulic models used to simulate the event.

Our study has four major objectives: i) to implement a hydrological and a hydraulic model in order to reproduce the October 2007 flash flood, ii) to validate the models through the comparison between model results and post-flood survey levels information, iii) to understand and decipher the flooding processes in alluvial fans systems using geomorphologic mapping, and in addition, iv) to provide information to improve flood risk management.

2. Study site

2.1. The Girona River basin

The Girona River basin is located in the Eastern part of the Iberian Peninsula, within the administrative territory of the Province of Alicante (Spain). The river flows through the Baetic Cordillera from west to east, along 32 km. The basin area at the river mouth into

126 the Mediterranean Sea is 117.7 km^2. The catchment encompasses various calcareous
127 mountains with a SW-NE orientation, separated by several corridors covered by
128 Miocene marls (Figure 1). The river is semi-ephemeral, and presents high transmission
129 losses, combining dry, intermittent and wet reaches.
130
131 The Girona River sources are located at 1300 m above the sea level. The river crosses
132 the Ebo Valley, a graben filled with tertiary marls, and downstream it flows through the
133 Laguar Valley, a deep calcareous canyon cut across Secondary deposits. This canyon
134 was used in 1945 to construct the Isbert Reservoir (capacity 1 Mm^3), now partially
135 silted and abandoned. Downstream, at the Retoria Valley, the alluvial plain starts to
136 widen. Two ephemeral tributaries (Bolata and Trullencs) cross this valley, parallel to the
137 Girona River. After crossing the town of Beniarbeig, the river built a large floodplain,
138 through the superposition of a complex sequence of alluvial fans made of Pleistocene
139 and Holocene deposits. Two ravines, Portelles and Alberca, also contributed to fill this
140 alluvial plain. To the north, the floodplain is flanked by the Segària Mountains, formed
141 by highly karstified Secondary limestone. To the south, various Tertiary hills close the
142 river floodplain (Vegas et al., 1975). The river flows into the Mediterranean at the
143 Almadrava cape. This floodplain has been largely urbanized during the last four
144 decades. The historical villages grew over the fans, terraces and point-bars, whereas
145 touristic residences were massively built on the coastal area. As a result of this, flood
146 vulnerability has enormously increased.
147
148 The climate in the area is Mediterranean. Mean annual rainfall is between 600 and 900
149 mm, with a maximum in autumn and a secondary peak in spring. Rainfall intensity in
150 this area is the highest of the Iberian Peninsula (Martin-Vide, 2004) and the maximum

accumulated rainfall in 24 hours is close to 1000 mm at some observatories neighbouring the Girona River (Armengot, 1994). Consequently, flash floods are frequent, particularly in October.

2.2. The October 2007 flood

The synoptic frame of the meteorological situation leading to the torrential rains of 11–12 October 2007 in the Valencia region was characterized by two phenomena: i) an easterly maritime wind advection across the Western Mediterranean, lasting for at least 48 hours, and ii) the presence of an upper-level isolated low over the Eastern Iberian Peninsula. The arrival of a moist air mass over the Valencia Region, and the presence of a cold pool aloft, caused torrential rainfall. The event was extensively described at the regional scale by Pastor et al. (2010).

The intense rainfall generated a flash flood, which affected the villages of Beniarbeig, El Verger and Els Poblets, and also the coastal urban area. At Beniarbeig, the CV-732 Bridge was destroyed. At El Verger, the flood was 2.4 m depth in some houses located on the river bank, and the river flow demolished a house and killed a woman. Most of the urban area of Els Poblets was also affected by the overbank flow.

According to Segura (2009), who analyzed 12 observatories belonging to the Automatic Hydrological Information System (AHIS) of the Jucar Basin Authority (JBA), rainfall varied between 250 and 420 mm. The highest intensities (> 150 mm/h) were recorded between 10:00 and 12:00 AM (12th October), particularly in the middle and upper basin

areas (Figures 2, 3a and 3b). Considering a mean catchment rainfall value of 343 mm, total rainfall was 35.2 Mm^3. Rainfall progressively increased from the coastline to the inland areas. The highest rainfall values were recorded within the mountain areas (420 mm), whereas in the coastal plain precipitation was between 250 and 300 mm.

The flood was generated in the headwaters area, and progressed towards the coastal area, supplied by the upper and middle basin tributaries. However, the low basin tributaries, such as Segària Mountains ravines, did not have relevant flow (Segura, 2009).

3. Materials and methods

This study combined hydrological and hydraulic modeling with geomorphology and post-flood survey in order to reproduce a particular flooding event and understand and decipher the flooding processes using geomorphologic mapping. First, the hydrological model TETIS (Francés et al., 2007) was used to estimate a range of possible hydrographs that represent the flood event of October 2007. Then, the range of hydrographs was simulated using free surface flow module of the model RiverFlow2D (Murillo and García-Navarro, 2010; Lacasta et al., 2014). The results were then validated using geomorphology and post-flood survey information to select the hydrograph that shows the best agreement between simulated and observed information. Finally, this combination of hydrological and hydraulic modeling and geomorphology was used to provide information to improve flood risk management.

3.1. Hydrological modeling

The flash flood of October 2007 was reconstructed by means of the hydrological model TETIS (Francés et al., 2007), a distributed conceptual hydrological model widely used in Spain and other countries (e.g. Bussi et al., 2012; Vélez et al., 2009). In this model, the main components of the hydrological cycle are represented by means of tanks. The TETIS model has a specific split-structure of the parameters (Francés et al., 2007) which allows its calibration without altering the spatial structure of the parameter maps. The model calibration can be carried out by adjusting up to nine correction factors, which multiply each a corresponding parameter map.

The Digital Elevation Model (5x5m resolution) was downloaded from the Spanish National Cartographic Centre (www.cnig.es). Nevertheless, the resolution of soil, geological and land use maps was larger. Therefore, the modelers' expertise and previous modeling work with the TETIS model led to increase the mesh size and resample the digital elevation model to 100x100 m as a compromise between model accuracy, resolution of the available information and computational time. The land-use map was obtained from the Corine Land Cover 2006 dataset, from the European Environment Agency (2007), while soil characteristic information was retrieved from local soil surveys and soil profiles. Geological maps were also used, obtained from the 1:50,000 geological maps of the Spanish Geological Institute. The soil retention capacity was computed as the difference between the soil water content at saturation and at the wilting point. These soil properties, as well as the soil infiltration capacity, were calculated depending on soil texture, organic content, soil structure and salinity according to Saxton and Rawls (2006)pedotransfer functions. The deep soil percolation

capacity was estimated based on literature values for the geological formations found in this catchment, depending on their lithology, degree of fracturing and macroporosity.

The rainfall of seven rain gauges within and surrounding the Girona River catchment (Gallinera, Isbert, Carrasca, Alcalalí, Guadalest, Algar and Azud de Mandem), with 5-minutes series, managed by the Jucar River Basin Authority (Confederación Hidrográfica del Júcar, CHJ) was used (Figure 2). The rainfall aggregation and interpolation was shown to be highly relevant in flash flood response and modeling (Borga et al., 2007; Anquetin et al., 2010; Nikolopoulos et al. 2011). In this study, the rain gauge station records were interpolated with a kriging technique, on a 1x1 km mesh and with a temporal resolution of 10 minutes. The spatial variations of the temperature were taken into account by assigning a value to each cell of the 100x100 m mesh depending on their distance from the meteorological stations, employing the Thiessen polygons methodology. No reliable water discharge records were available for the Girona River catchment. For this reason, a nearby similar catchment was used to implement the model: the Guadalest reservoir (54.34 km^2 drainage basin area). The TETIS model was calibrated for the October 2007 event (the event to be reconstructed), by adjusting its model parameters, and validated for three other rainfall events (April 2003, October 2008 and September 2009) for the same station.

No evapotranspiration data was available for this study. This is a key variable in flash flood modeling (Braud et al., 2010; Vannier et al., 2013) because it determines the wetness of the catchment soils at the beginning of the flood. The soil characteristics and their relationships with soil saturation dynamics are acknowledged to be a key issue in the formation of flash floods in several studies (Braud et al., 2014, 2010; Nikolopoulos

et al., 2011; Norbiato et al., 2008). For these reasons, and given the lack of precise evapotranspiration data, we decide to implement the model at the event scale. This means that the initial values of the model state variables cannot be initialized by means of a warm-up simulation and must be calibrated along with the model parameters. In particular, the initial value of the soil static storage, which is a model state variable related to soil wetness, is a key variable for flash flood modeling, and must be calibrated carefully. The initial soil storage of the calibration event (October 2007) and validation events (April 2003, October 2008 and September 2009) was adjusted along with the model parameters in order to reproduce the observed hydrograph at the Guadalest reservoir.

The model calibrated and validated at the Guadalest catchment was used to reproduce the October 2007 hydrograph of the Girona River upstream of the flood plain (indicated as the hydraulic model area in Figure 1). This was done by running the TETIS model for the Girona River catchment with the parameterization obtained from the Guadalest catchment. This process of extrapolation from a gauged catchment to an ungauged one is widely used in distributed hydrological modeling (Vélez et al., 2009), and it is known to amplify the uncertainty of the model result. For this reason, we used the extrapolated model results to obtain only the hydrograph shape, while the actual magnitude of the Girona River hydrograph was obtained by calibrating the initial soil storage and using post-flood information as a reference. In particular, the initial soil storage was modified within a reasonable range in order to obtain a set of hydrographs with the same shape but different peak flows and volumes, which were used as boundary condition for a flood model. A flood simulation was run with each of these hydrographs, the resulting water depth maps were compared with post-flood information similarly to what was

done by Braud et al. (2010), and the simulation providing the best fit was selected. This was done by comparing visually the observed and simulated flood zone. The final October 2007 reconstructed hydrograph was the one returning the best fit between observed and simulated inundation map and flood depths.

3.2. Hydraulic modeling

The set of hydrographs produced by the hydrological model were used as inlet discharge to simulate the flooding event at the floodplain of the Girona River (Figure 1). To that end, the free surface flow module of the model RiverFlow2D (Murillo and García-Navarro, 2010; Lacasta et al., 2014) was used.

3.2.1. Hydraulic model

The 2D Shallow Water Equations, which express the water volume and momentum conservation in *x* and *y* directions, were used in this work (Eq. 1):

$$\frac{\partial}{\partial t}\begin{pmatrix} h \\ hu \\ hv \end{pmatrix} + \begin{pmatrix} hu \\ hu^2 + \frac{1}{2}gh^2 \\ huv \end{pmatrix} + \frac{\partial}{\partial y}\begin{pmatrix} hv \\ huv \\ hv^2 + \frac{1}{2}gh^2 \end{pmatrix} = \begin{pmatrix} 0 \\ -gh\left(\frac{\partial z}{\partial x} + S_{fx}\right) \\ -gh\left(\frac{\partial z}{\partial y} + S_{fy}\right) \end{pmatrix} \quad (1)$$

Where *h* is the water depth, (*u*, *v*) are *x* and *y* averaged velocity components respectively, *z* is the bottom level and the friction losses are written in terms of Manning's roughness coefficient (*n*) (Eq. 2):

299 $S_{fx} = \frac{n^2 u\sqrt{u^2+v^2}}{h^{4/3}}, S_{fy} = \frac{n^2 v\sqrt{u^2+v^2}}{h^{4/3}}$ (2)

300

301 In order to solve the system of equations, an upwind cell-centered finite volume model
302 was applied (Toro, 2001, Murillo and García-Navarro, 2010).The domain was
303 discretized into triangular cells and, assuming a piece wise representation of the
304 variables, an explicit first order Godunov method based on Roe's approach was
305 considered (Roe, 1981, Murillo and García-Navarro, 2010) (Eq. 3):

306

307 $U_i^{n+1} = U_i^n - \frac{\Delta t}{A_i}\sum_{k=1}^{NE}\sum_m^3 \left[\left(\tilde{\lambda} - \tilde{\gamma}\tilde{e}\right)_k^m l_k\right]^n$ (3)

308

309 where U= (h, hu, hv) is the vector of conserved variables, *NE* indicates the number of
310 edges in cell i, l_k is the length of each edge k, λ and $\tilde{e}$ are the eigenvalues and
311 eigenvectors of the Jacobian matrix, respectively, and γ accounts for the linearized
312 fluxes and source terms expressed compactly (Morales-Hernández et al. 2013).
313 Moreover the numerical method was implemented in GPU architectures in order to
314 accelerate the computations. More information can be found in Lacasta et al. (2014).

315

316 3.2.2. Topography

317

318 A Digital Terrain Model (DTM) of 1x1 m resolution derived from LiDAR (Light
319 Detection and Ranging) data was used as base information to perform the final domain
320 discretization. LiDAR data was collected in 2009 by the PNOA (The National Plan of
321 Aerial Ortophotogrammetry, Government of Spain), using an Optech ALS50-II sensor,
322 with a minimum laser pulse rate frequency of 45 kHz, a field of view angle of 50º and a
323 scan rate of 70 Hz. The final density ranged between 0.5 (most of the area) and 2

points/m^2(flight overlapping). Reported vertical and planimetric (X,Y) errors were lower than 40 and 36 cm, respectively. Then, a Digital Elevation Model (DEM)was performed using ground returns in Fusion software v3.30 (McGaughey, 2009). Likewise, a building map was carried out using the building returns in Fusion software v3.30 (McGaughey, 2009). Both models were combined to perform the DTM.

However, the following modifications of the DTM were carried out in order to represent accurately the simulated domain: i) as the LiDAR does not represent the terrain behind the bridges, this task was carried out manually using the nearest neighbour interpolation of ArcGis9.3 software (ESRI, Redlands CA); ii) some buildings were removed from the building map as they did not exist in 2007; iii) agricultural walls and irrigation infrastructures were also modified in order to represent the terrain of 2007. Besides, some of them were not accurately reproduced by LiDAR data, and were manually introduced; and iv) riverbanks, gravel bars and ripraps were also modified according to the topography of 2007. Finally the modified DTM is discretized to perform an unstructured triangular mesh with 1,858,396 cells.

The roughness of the domain was defined depending on the land use, which was obtained from the Corine map (European Environment Agency, 2007).The Manning roughness coefficient was assigned to each habitat according to the recommendations found in the specialized bibliography (i.e. Chow, 1959; Acrement and Schenider, 1990; Rhee et al., 2008; González-Sanchis et al., 2012).

The inlet boundary condition is the hydrograph derived from the hydrological model. On the contrary, the only outlet boundary condition is that of the sea level, which was established following the tidal levels suggested by GIOC (2001).

3.3. Geomorphology and post-flood surveys

3.3.1. Geomorphologic works.

A geomorphologic survey of the study area was developed in order to assess and validate flood processes. This task was based on field reconnaissance along the river and throughout the whole Girona floodplain. Panchromatic black-and-white aerial photographs dating from 1946 and 1956 (Ministry of Defense, CECAF) were used to identify forms recently transformed by the urbanization processes. The photographs were scanned at a resolution of 400 dpi to obtain average pixel dimensions of 1 m and 1.15 m respectively, and they were georeferenced to orthophotos using ArcGIS TM version 9.3 (ESRI, Redlands, CA, 2009). The LiDAR-based DEM performed for hydraulic modeling was also used for geomorphologic analysis.

3.3.2. Flooded area

The mapping of the flooded area was obtained from two different sources. First, some days after the flood, the external edge of the flooded area was surveyed using GPS. These data were exported to .shp format to be processed with ArcGIS TM version 9.3 (ESRI, Redlands, CA, 2009). This information was compared with a map composed by

372 the Plataforma Ciutadana Riu Girona (PCRG) association. This organization was
373 created by some citizens affected by the October 2007 flood, in order to promote
374 research on this river basin and to prevent future floods. The PRG collected information
375 from both local administrations and witnesses to map the evolution of the flood, which
376 was simulated through a video (PCRG, 2009, https://vimeo.com/5487707). Some small
377 discrepancies were found between the GPS mapping and the PCRG video-mapping.
378 Part of them was solved after visiting the area and consulting some members of the
379 PCRG and other interviewed witnesses. Finally, the flooded area between Beniarbeig
380 and El Verger was selected for validation, because it did not present significant
381 discrepancies between the two sources and reproduced with the highest precision the
382 flooding event (Figure 4).
383
384 3.3.3. Maximum flood depths.
385
386 The day after the flood, some technicians from the municipality of El Verger visited all
387 the buildings affected by the flood, in order to produce an assessment to be used to
388 calculate economic compensations for damages. Flood levels recorded by this report
389 were compared with flood marks observed in pictures taken by the authors or included
390 in the report, in order to correct some over-dimensioned records. A total of 64 points
391 with a register of the maximum flood depth were used to validate the performance of
392 the hydrological and the hydraulic model. These data are limited to the town of El
393 Verger, which represents only a small fraction of the total flooded area (Figure 4).
394
395 3.4 Validation of the simulated flooding event.
396

The results of the hydrological and hydraulic model was validated using the post-flood surveys: maximum flooded area and flood depth. The observed maximum flood extension was compared to the estimated one following Bates and De Roo (2000) criteria, in which where the accuracy of the calculated flood extent versus the observed is defined on:

$$\mathrm{Fit}_A(\%) = \frac{\mathrm{FAobs} \cap \mathrm{FAmod}}{\mathrm{FAobs} \cup \mathrm{FAmod}} \mathrm{x}\ 100 \quad (4)$$

Where FIT_A is a goodness-of-fit index, and *FAobs* and *FAmod* are the observed and modelled flooded areas respectively. The observed and simulated maximum flood depths at the 64 points of El Verger are compared using the following goodness-of-fit indexes: Root Mean Square Error (RMSE) and Nash and Sutcliffe Efficiency - NSE (Nash and Sutcliffe, 1970).

3.5. Hydro-geomorphologic response to model simulations

Simulations varying flow conditions, with peak flows ranging from 200 $m^3\ s^{-1}$ to 900 $m^3\ s^{-1}$ with intervals of 100 $m^3\ s^{-1}$ were carried out to estimate the hydro-geomorphologic response of the Girona River floodplain. The aim of these simulations was to identify the threshold of activation for different geomorphic elements: alluvial fans, inter-fan depressions, palaeochannels and tectonic depressions, and to analyse the flood risk (and how to prevent it) within the study area.

420 4. Results

421

422 4.1. Hydrological modeling

423

424 The hydrological model TETIS was calibrated at the Guadalest Reservoir flow gauge,
425 by comparing the predicted and the observed water discharge. As explained in the
426 methodology section, given that the model was implemented at the event scale, the
427 initial state of soil moisture was unknown and was also calibrated. The results are
428 shown in Figure 5. The model provided a NSE of 0.88 (Francés *et al*. 2011). The model
429 was temporally validated on different events, showing NSE of 0.88, 0.92 and 0.91 for
430 the April 2003, October 2008 and September 2009 events respectively, providing
431 satisfactory results. More information about the TETIS model implementation can be
432 found in Francés et al. (2011), CHJ (2012) and Bussi et al. (2012).

433

434 The October 2007 hydrograph of the Girona River was reconstructed using TETIS. A
435 set of 26 hydrographs was generated (Figure 6) varying the initial soil storage from 35%
436 to 60%, and it was used as the input of the flood model.

437

438 Table 1 – Characteristics of the reconstructed flood event (October 2007) for the Girona
439 River catchment, following the results of the hydrological model.

440

Total precipitation – catchment average (mm)	343
Max rainfall intensity – catchment average (mm h^{-1})	69.5
Total rainfall volume (catchment) at the hydraulic model inflow section (Mm^3)	35.2
Total hydrograph volume (Mm^3)	11.2

Proportion of overland flow to total rainfall (%)	15.5
Proportion of interflow to total rainfall (%)	16.7
Maximum discharge ($m^3 s^{-1}$)	515
Unit discharge ($m^3 s^{-1} km^{-2}$)	0.58
Unit peak discharge ($m^3 s^{-1} km^{-2}$)	5.0
Runoff coefficient (%)	31.9

441

442 The observed precipitation series showed two rainfall peaks. The first occurred between
443 10:00 and 10:45, with maximum intensity over 100 mm h^{-1} in the headwaters (Ebo
444 Valley). The second took place between 11:15 and 11:45 in the central part of the
445 catchment, mainly at the southern part of Laguar Valley. Again, the rainfall intensity
446 was above 100 mm h^{-1}. The average hyetographs describes well both peaks, with
447 intensities above 69.5 mm h^{-1}.

448

449 According to the hydrological model results, the discharge at the catchment outlet
450 (hydraulic model inflow) started to rise at 8:30AM (12th October) and reached a peak at
451 13:00 (515 $m^3 s^{-1}$). The hydrograph lag-time was established as the difference in time
452 between the precipitation peaks (11:20 at Isbert and Carrasca and 11:40 at Alcalalí and
453 Gallinera) and the peak discharge time. That provides a lag time of 1h20 – 1h40, which
454 is typical for flash floods in similar catchments (Camarasa and Segura, 2001) and
455 slightly higher than those estimated by Marchi et al (2010).

456

457 The hydrograph lasted two days, although the largest discharges (above 100 $m^3 s^{-1}$) only
458 took place during 8 hours and 40 minutes. Using the methodology detailed in Salazar et
459 al. (2013), the peak discharge return period was estimated to be 40 years, while the

460 expected return period of daily rainfall was estimated to be slightly lower than 50 years.
461 As expected, the single rainfall burst observed produced a single discharge peak. A
462 second and smaller rainfall burst took place at 19:30 and produced a relatively reduced
463 discharge peak (150 $m^3 s^{-1}$) at 21:00, repeating the 1-2 h lag time observed above.
464
465
466 4.2. Hydraulic modeling
467
468 The set of 26 hydrographs generated with the hydrological model varying the initial soil
469 storage from 35% to 60% was used as input to the hydraulic model. The simulation
470 results were analysed according to the post-flood survey information available and the
471 geomorphology. Following this analysis, the hydrographs derived from the initial soil
472 storage between 35 and 40 % showed a simulated flooded area smaller than the
473 observed one and a lack of hydraulic conductivity at the palaeochannels P3 and P4 (see
474 Figure 8). Likewise, initial soil storages higher than 45 %, produced an activation of the
475 P7 palaeochannel (see Figure 8) that did not occur during the flood of October 2007.
476 Thus, the hydrographs obtained with initial soil storages between 35 and 40 %, and
477 between 46 and 50 % were dismissed.
478
479 In order to select only one hydrograph that represented the flood of October 2007, the
480 results of the hydrographs with initial soil storage between 41 and 45 % were analysed
481 in detail by comparing the simulated and the observed maximum flooded area and flood
482 depth (see Table 2). The comparison showed a good agreement between observed and
483 simulated flooded area for the five hydrographs, whose Fit_A varied from 75.3 to 76.4 %
484 (see Table 2). Likewise, the flood depth showed an acceptable accuracy, with a NSE

485 and RMSE that ranged between 0.58-0.61 and 0.64-0.69, respectively (see Table 2). All
486 five hydrographs accurately reproduced the flooded area. However, the best
487 compromise between flooded area and flood depth accuracy was that provided by the
488 hydrograph generated with initial soil storage of 44 % (see Table 2 and Figure 7). Thus,
489 according to the combination between hydrological and hydraulic modeling with post-
490 flood information it can be stated that the flash flood occurred in October 2007 at the
491 Girona River reached a peak discharge of 515 $m^3 s^{-1}$.
492
493 Table 2.Results of the comparison between observed and estimated maximum flood
494 depth (NSE and RMSE) and maximum flooded area (Fit_A) using the hydrographs
495 derived from the initial soil storage between 41 and 45 %.
496

Initial soil storage (%)	**41**	**42**	**43**	**44**	**45**
NSE	0.58	0.59	0.59	0.60	0.61
RMSE	0.69	0.68	0.66	0.65	0.64
Fit_A	75.61	76.13	76.39	76.14	75.28

497
498
499 4.3. Floodplain geomorphologic configuration
500
501 The Girona floodplain is made of a complex sequence of Quaternary alluvial deposits,
502 developed by the Girona River and the Alberca and Portelles Ravines. Middle
503 Pleistocene sediments are present at the inner part of the floodplain, whereas Late
504 Pleistocene and Holocene fans are located towards the coastline. This system of
505 overlapped prograding alluvial fans, palaeochannels and inter-fans depressions are
506 characteristic of Valencian coastal plains and they have a determinant influence on

flood hazard assessment (Segura, 2003). Overbank flow usually takes place at the apex of alluvial fans and the flooding areas are located at palaeochannels, inter-fan depressions and tectonic depressions, as well as marshes. In the study area, several morphological units have been identified:

i) Structural depression of Clot del Francés

This rectangular depression, parallel to the Girona River and the Segària Mountains, has a probably tectonic origin (Figure 8). In fact, some raised and down-dropped Miocene blocks were identified in the coastal plain (Vegas et al., 1975). The depression creates a corridor which is determinant for flooding processes, because it concentrates part of the overbank flow coming from the western river bank. The Cremadella Ravine, which also flows into this corridor, forms a small torrential fan (F7) at the western side of the Clot del Francés depression (Figure 8).

ii) Girona overlapped prograding fans

Downstream Beniarbeig, where the river valley widens, numerous avulsion processes created a complex system of prograding alluvial fans, with different palaeochannels (Figure 8). The older fan is located at the right river bank (F1), oriented to the southeast, and it has a long palaeochannel (P1) which could have connected the Girona River with the Alberca Ravine streambed in the past (Figure 8). There are other two palaeochannels at the left bank (P3 and P4), which go down the Clot del Francés depression.

Immediately downstream, there is a dissymmetric fan (F2), which is well developed at the right bank, but almost unrecognizable in its left side. This is due to the probable subsidence of the Clot del Francés area, subsequent to fan development.

At the distal area of this fan (F2), two more recent alluvial fans (F3 and F4) were constructed. The first one (F3) comes from a 90º meander, where the rivers twists to the East, leaving to palaeochannels to the left (P5 and P6). At this point, there is a crevasse splay, clearly marked in the micro-topography, which presents an accumulation of boulders transported by the 2007 flood. The second one (F4) lies on the right and it is flanked by another palaeochannel (P7). These fans (F3 and F4) are overlapped by another two (F5 and F6), the last one of which forms the triangular shaped protuberance of the Almadrava Cape.

iii) Alberca and Portelles fans

Girona River fans coalesce with deposits formed by the Portelles and Alberca ravines (Figure 8). During floods, palaeochannels can connect these systems. In fact, during the event in 2007, flow from the Girona River was partially drained by the Portelles channel.

The Portelles Ravine forms a small torrential fan at the foot of the Segària mountain (F8). At the connection with the Clot del Francés palaeochannel (P3), there is a wide fan, built with Girona materials, in contact with the Pego-Oliva wetland. In its last reach, the channel almost completely vanishes, and leaves a dejection cone (F10) on this coastal marsh.

The Alberca Ravine flows attached to several Miocene hills. It has also constructed an alluvial fan (F11) in its lower reach. Due to the convexity of the fan surface, an inter-fan depression is formed between the Alberca (F11) and Girona (F2, F4), which can concentrate the overbank flow from both channels.

4.4. Flooding thresholds for morphological units

Hydro-geomorphological responses for different flow conditions were estimated through various simulations. Results (Table 3, Figure 9) showed a geo-chronological activation sequence for palaeochannels and alluvial fans, altered by the Clot del Francés depression (P7) and the impact of the CV-729 Bridge.

Table 3. Flooding thresholds for geomorphologic units

Flow ($m^3 s^{-1}$)	Effects	Fans Activation
200	No impact on point-bars or palaeochannels. Overbank flow at river mouth meander, immediately upstream F6.	F6 (Holocene)
300	Point-bars flooding. P5 and P6 initial activation.	F3 (Late Pleistocene)
400	P3 (Clot del Francés) activated. Initial overbank flow at P4. Overbank flow at F5 apex over F4 distal area.	F5 and F4(Late Pleistocene)
515	Optimal coincidence between flooded area and hydraulic model.	F10 (Holocene, Portelles Ravine)

527	P7 initial activation.	F4(Late Pleistocene)
592 - 600	P7 active. Overbank flow from F4 apex also flooding the inter-fan depression.	F9 (Late Pleistocene, Portelles Ravine)
700	Overbank flow on the right side of CV-729 Bridge.	F2 (Late Pleistocene)
900	Overbank flow at Beniarbeig and AP7 motorway creating stagnation effect.	Middle Pleistocene Bajada

571

572

573

574 5. Discussion

575

576 The hydrological model provided a unit peak discharge of 5.0 $m^3 s^{-1} km^2$. According to
577 Gaume et al. (2009), this is a rather high unit peak discharge. For the Spanish
578 Mediterranean, Gaume et al. (2009) found a maximum unit peak discharge of around 10
579 $m^3 s^{-1} km^2$ for a 100 km^2 catchment. The Girona River unit peak discharge for the
580 October 2007 event is also within the range of peak discharge data collected by Marchi
581 et al. (2010). The ratio of the unit peak discharge (5 $m^3 s^{-1} km^{-2}$) and the unit average
582 discharge (0.58 $m^3 s^{-1} km^{-2}$) is 8.65. These values compares well with the extreme flash
583 floods described by Gaume et al. (2009) and Marchi et al. (2010) for Mediterranean
584 catchments. Given the outcomes of these studies, the October 2007 can be classified as
585 an extreme rainfall event whose magnitude is very close to the unit peak discharge
586 envelope curve showed by Gaume et al. (2009) and Marchi et al. (2010).

587

588 In this study, we calculated a runoff coefficient of 31.9% (Table 1). This is similar to
589 what found by Marchi et al. (2010). These authors analysed 25 flash floods in Europe
590 and found that the mean value is 0.35, with standard deviation equal to 0.18, median
591 value 0.37 and 0.20-0.45 interquartile range. However, the value found in the present
592 study is substantially higher than the runoff coefficients found by Goodrich (1990) who
593 analysed five large flash floods events at the semi-arid catchment of Walnut Gulch (US)
594 occurred within a 20-year period and found runoff coefficients between 0.07 and 0.21.
595 Segura (1990) and Camarasa and Segura (2001) in other limestone catchments of the
596 Valencia region found that, for a 25-year time series and 35 floods, the runoff
597 coefficients are between 0.007 and 0.16. These values, observed in karstified limestone
598 catchments, indicate that the infiltration is relatively high, as well as the initial
599 abstractions and the soil retention. The catchments can infiltrate a large amount of
600 water, and when they are saturated they produce a sudden pulse of runoff (Camarasa
601 and Segura, 2001).
602
603 Simulated and observed maximum flooded area and flood depth were compared in order
604 to adjust the hydrograph. This comparison showed the accuracy of the model predicting
605 the maximum flooded area (see Table 3), which is a good test of model capabilities and
606 is of a significant practical interest (Bates and De Roo, 2000). The goodness-fit
607 indicator Fit_A reached 76.14 %, and is similar to that reported by González-Sanchis et
608 al. (2012) using the same hydraulic model, which ranged from 64 to 92 %. The resulted
609 accuracy is also comparable to other studies, such as Horritt and Bates (2001), who
610 obtained a FitA = 0.84% using the TELEMAC-2D hydraulic model and satellite
611 imagery data for the validation step. However, this comparison should be carefully
612 interpreted as Horritt and Bates (2001) only simulated a steady-state flow peak and the

satellite imagery data are less accurate than our validation data. Likewise, Tayefi et al.(2007) reported a Fit_A that ranged from 51 to 65 % using a 2D diffusion wave hydraulic model and surveyed wrack lines measured on the day after the flood event as a validation data.

Regarding the validation of the maximum flood depth, the results showed an acceptable accuracy, although slightly lower than the one reported in other studies. Connell et al. (2001), reported ±0.26 m Standard Error in water depth using HYDRO-2D model and resident-supplied information and photographs for the validation purpose. Erpicum et al. (2010) obtained a difference between measured and calculated water depth that ranged from 0.01 to 0.25 m using a 2D hydraulic model based similar to the one used in this study. Buttner et al. (2006) reported a difference between measured and calculated water depth that ranged from 0.1 to 0.40 m using the hydraulic model RMA-2. However, the lower accuracy registered in this study could be due to the fact that none of these studies simulate the whole flooding event, but only steady-state peak flows. González-Sanchis *et al* (2012) simulated five transient flooding events using the same hydraulic model and obtained a difference between measured and computed flood depth between 0.16 and 0.36 m, which is slightly lower than the one reported in this study. Thus, the lower accuracy might not only be due to the transient characteristics of the simulated flood, but also to the high complexity of the case. Unlike the cited studies, this study is highly complex in terms of simulation and validation, as the Girona River is ephemeral, ungauged, the inlet discharge was estimated from a hydrological model and the outlet discharge was unknown.

With regard to the flooding processes, alluvial fan systems have flood-hazardous conditions due to their convex topography, which creates high flow direction uncertainty downstream the intersection point (fan apex). The determination of the active zone (area where flooding, erosion, and sedimentation are possible) of these alluvial forms is a complex task, which can be solved with the combination of hydrologic, hydraulic and geomorphologic techniques. Several authors have addressed this topic with different approaches. Santangelo et al. (2012), in their analysis of fan systems, considered as active zone all the fan portions located down-fan of the intersection point. This is consistent with the NRC (1996) recommendations, which followed a geo-chronological criterion, considering the Holocene fans as the most active zones.

Moreover, Segura (2003) showed that, in the Valencia Region coastal plains, the topographic complexity of alluvial fans structure requires a more detailed analysis, in order to discriminate between morphological units with different flood-hazard. In these contexts, the activation of palaeochannels and the presence of inter-fan depressions play a major role during flood events. During the Girona 2007 flash flood, palaeochannels conveyed an important proportion of the overbank flow, preventing other areas of the alluvial fans from flooding, as it was shown in the real event and model simulations. Besides, inter-fan depressions should be also considered as active zones, due to its capability to drain flow from both the fan distal areas and the palaeochannels, as it is shown in simulations with stream flow > 600 m3 s-1.

In this work, the simulation of different flow conditions showed various thresholds for fans flooding and palaeochannels activation (Figure 9). The lower flooding thresholds

662 were located both at the point-bar areas and the Holocene fan (F6). Intersection points
663 and palaeochannels located in the Late Pleistocene fans (F2, F3, F4, F5, F9 and F10)
664 were activated in the following flow thresholds. The inactivity of the Middle
665 Pleistocene fan and palaeochannels revealed the existence of a geo-chronological
666 activation pattern. Only the Middle Pleistocene bajada in Beniarbeig was activated
667 during the maximum flow simulations calculated (900 m^3 s-1).
668
669 This geo-chronological sequence was uniquely altered in the study area by two effects:
670 i) the topographic anomaly generated by the tectonic depression of Clot del Frances,
671 activating the P3 and P4 palaeochannels, and ii) the effect of the CV-732 bridge, which
672 artificially narrows the river section, prematurely activating the P4 palaeochannel and
673 also causing unexpected overbank flow on the right (eastern) bank beyond the 700 m^3 s^{-1}
674 . This is actually the only case of overbank flow inconsistent with the geomorphologic
675 expected response, being a clear consequence of anthropogenic action.
676
677 In this regard, the urban use of some of these morphologies is considerably increasing
678 flood vulnerability in the area. While the older part of urban areas (previous to 1950)
679 were in most cases not affected by the 2007 flash flood, recent constructions occupy
680 sensitive zones such as point-bars or palaeochannels. Moreover, the massive occupation
681 of the coastal front blocks the flow descending to the Sea. For these reasons, the role
682 played by the Clot del Frances palaeochannel (P3) during this flash flood and the
683 simulated scenarios demands the preservation of this area, free of constructions, for
684 flood attenuation.
685
686

6. Conclusions

The analysis of the flash flood of the Girona River in 2007 has reconstructed the flooding susceptibility of this Mediterranean alluvial floodplain. From a methodological point of view, this integrated perspective appears to be a useful strategy for ungauged drainage basins. The combination of hydrologic and hydraulic modeling, and geomorphologic information allows understanding and generalizing the mechanisms governing floods in alluvial fans.

The implementation of both hydrologic and hydraulic models was complex in terms of simulation and validation, as this river is ephemeral and ungauged, but results are consistent with similar works. The interaction of the hydraulic model with the geomorphologic information was determinant to decipher flooding processes and to provide a better understanding of overlapping alluvial fan systems response. Results from this multidisciplinary research are a useful tool to perform risk prevention works and may be effectively used by the public administrations for early warning and risk mitigation purposes.

Acknowledgements

This collaborative research was financed with the projectsCGL2013-44917-Rand SLWAMED CGL2014-58127-C3-2, of the Ministry of Economy and Competitiveness of the Spanish Government. Both projects were co-financed with FEDER funds. The observed rainfall and water discharge records were provided by “Sistema Automático

de Información Hidrológica (SAIH)", which belongs to the CHJ (Spain). This work was also possible due to the kind cooperation of the members of the Plataforma Ciutadana Riu Girona and several anonymous farmers interviewed during the field works.

References

Acrement, G. C., Schenider, V. R. 1990. Guide for selecting Manning's roughness coefficients for natural channels and flood plains. Water-Supply Paper No. 2339, Dept. of the Interior, U. S. Geological Survey, Reston, VA.

Anquetin, S., Braud, I., Vannier, O., Viallet, P., Boudevillain, B., Creutin, J.D., Manus, C., 2010. Sensitivity of the hydrological response to the variability of rainfall fields and soils for the Gard 2002 flash-flood event. J. Hydrol. 394, 134–147. doi:10.1016/j.jhydrol.2010.07.002

Armengot, R., 1994. Les precipitacions extraordinàries, in Pérez Cueva, A. (coord.) Atlas Climàtic de la Comunitat Valenciana, COPUT, Generalitat Valenciana, Valencia, pp. 98-99.

Barredo, J.I., 2007. Major flood disasters in Europe: 1950–2005. Natural Hazards 42, 125–148.

Barrera, A., Llasat, M., Barriendos, M., 2006. Estimation of extreme flash flood evolution in Barcelona County from 1351 to 2005. Natural Hazards and Earth System Science. 6, 505-518.

735 Bates, P. D., De Roo, A. P. J. 2000. A simple raster-based model for flood inundation
736 simulation. Journal of hydrology, 236(1), 54-77.

737 Bates, P.D., Wilson, M.D., Horritt, M.S., Mason, D.C., Holden, N., Currie, A., 2006.
738 Reach scale floodplain inundation dynamics observed using airborne synthetic aperture
739 radar imagery: Data analysis and modelling. J. Hydrol. 328, 306–318.
740 doi:10.1016/j.jhydrol.2005.12.028

741 Borga, M., Anagnostou, E. N., Blöschl, G., & Creutin, J. D.,2011. Flash flood
742 forecasting, warning and risk management: the HYDRATE project. Environmental
743 Science & Policy, 14(7), 834-844.

744 Borga, M., Boscolo, P., Zanon, F., Sangati, M., 2007. Hydrometeorological Analysis of
745 the 29 August 2003 Flash Flood in the Eastern Italian Alps. J. Hydrometeorol.
746 doi:10.1175/JHM593.1

747 Borga, M., Morin, E., 2014. Characteristics of Flash Flood Regimes in the
748 Mediterranean Region, in: Diodato, N., Bellocchi, G. (Eds.), Storminess and
749 Environmental Change Climate Forcing and Responses in the Mediterranean Region.
750 Springer Dordrecht Heidelberg New York London, pp. 65–76. doi:10.1007/978-94-007-
751 7948-8_5

752 Braud, I., Roux, H., Anquetin, S., Maubourguet, M.M., Manus, C., Viallet, P., Dartus,
753 D., 2010. The use of distributed hydrological models for the Gard 2002 flash flood
754 event: Analysis of associated hydrological processes. Journal of Hydrology. 394, 162-
755 181. doi:10.1016/j.jhydrol.2010.03.033.

Braud, I., Ayral, P.-A., Bouvier, C., Branger, F., Delrieu, G., Le Coz, J., Nord, G., Vandervaere, J.-P., Anquetin, S., Adamovic, M., Andrieu, J., Batiot, C., Boudevillain, B., Brunet, P., Carreau, J., Confoland, A., Didon-Lescot, J.-F., Domergue, J.-M., Douvinet, J., Dramais, G., Freydier, R., Gérard, S., Huza, J., Leblois, E., Le Bourgeois, O., Le Boursicaud, R., Marchand, P., Martin, P., Nottale, L., Patris, N., Renard, B., Seidel, J.-L., Taupin, J.-D., Vannier, O., Vincendon, B., Wijbrans, A. 2014. Multi-scale hydrometeorological observation and modelling for flash-flood understanding. Hydrology and Earth System Sciences, 18(9), 3733-3761.

Bussi, G., Francés, F., Salinas, J.L., García-Bartual, R., Pujol, L., Ortíz, E., 2012. Estimación de mapas de peligrosidad mediante generación de tormentas sintéticas, in: Murillo Muñoz, R.E. (Ed.), XXV Congreso Latinoamericano de Hidráulica. Colegio de Ingenieros Civiles de Costa Rica, San José, Costa Rica.

Büttner, O., Otte-Witte, K., Krüger, F., Meon, G., Rode, M., 2006. Numerical modelling of floodplain hydraulics and suspended sediment transport and deposition at the event scale in the middle river Elbe, Germany. Acta Hydrochim.Hydrobiol. 34, 265-278.

Camarasa Belmonte, A.M., Segura Beltrán, F.S., 2001. Flood events in Mediterranean ephemeral streams (ramblas) in Valencia region, Spain. Catena. 45 (3), 229-249.

Camarasa-Belmonte, A.M., Soriano-García, J., 2012. Flood risk assessment and mapping in peri-urban Mediterranean environments using hydrogeomorphology. Application to ephemeral streams in the Valencia region (eastern Spain). Landscape Urban Plann. 104, 189-200. doi: 10.1016/S0341-8162(01)00146-1.

778 Confederación Hidrográfica del Júcar (CHJ), 2012. Plan director de defensa contra las
779 avenidas en la comarca de la Marina Alta (Alicante). Apendice 6. Estudio hidrológico.
780 Jucar River Basin Authority.

781 Chow, V.T., 1959. Open-channel hydraulics, New York, McGraw-Hill, 680.

782 Connell, R.J., Painter, D.J., Beffa, C., 2001. Two-dimensional flood plain flow. II:
783 Model validation. J.Hydrol.Eng. 6, 406-415.

784 Creutin, J. D., Borga, M., Gruntfest, E., Lutoff, C., Zoccatelli, D., & Ruin, I. (2013). A
785 space and time framework for analyzing human anticipation of flash floods. Journal of
786 Hydrology, 482, 14-24.doi:10.1016/j.jhydrol.2012.11.009

787 Di Baldassarre, G., Schumann, G., Bates, P.D., 2009. A technique for the calibration of
788 hydraulic models using uncertain satellite observations of flood extent. Journal of
789 Hydrology. 367, 276-282. doi:10.1016/j.jhydrol.2009.01.020.

790 Erpicum, S., Dewals, B., Archambeau, P., Detrembleur, S., Pirotton, M., 2010. Detailed
791 inundation modelling using high resolution DEMs. Engineering Applications of
792 Computational Fluid Mechanics. 4(2), 196-208.

793 European Environment Agency (EEA), 2007. CLC 2006 technical guidelines. EEA
794 Technical Report No 17/2007. European Environment Agency, Copenhagen.

795 Francés, F., Velez, J.I., Vélez, J.J., 2007. Split-parameter structure for the automatic
796 calibration of distributed hydrological models. Journal of Hydrology. 332, 226-240.
797 doi:10.1016/j.jhydrol.2006.06.032.

798 Francés, F., Garcıa-Bartual, R., Bussi, G., 2011. High return period annual maximum
799 reservoir water level quantiles estimation using synthetic generated flood events. Risk
800 Analysis, Dam Safety, Dam Security and Critical Infrastructure Management. Taylor &
801 Francis Group, London, 185-190.

802 Gaume, E., Bain, V., Bernardara, P., Newinger, O., Barbuc, M., Bateman, A.,
803 Blaškovičová, L., Blöschl, G., Borga, M., Dumitrescu, A., Daliakopoulos, I., Garcia, J.,
804 Irimescu, A., Kohnova, S., Koutroulis, A., Marchi, L., Matreata, S., Medina, V.,
805 Preciso, E., Sempere-Torres, D., Stancalie, G., Szolgay, J., Tsanis, I., Velasco, D.,
806 Viglione, A., 2009. A compilation of data on European flash floods. Journal of
807 Hydrology. 367, 70-78. doi:10.1016/j.jhydrol.2008.12.028.

808 Gaume, E., Borga, M. (2008). Post-flood field investigations in upland catchments after
809 major flash floods: proposal of a methodology and illustrations.*Journal of flood risk*
810 *management*, *1*(4), 175-189.doi:10.1111/j.1753-318X.2008.00023.x

811 GIOC, 2001. Atlas de inundación del litoral peninsular español. Grupo de Ingeniería
812 Oceanográfica y de Costas, Universidad de Cantabria (Spain) - Ministerio de Medio
813 Ambiente, Dirección General de Costas (Spain).

814 Godunov, S.K., 1959. A difference method for numerical calculation of discontinuous
815 solutions of the equations of hydrodynamics. Matematicheskii Sbornik. 47 (89), 271-
816 306.

817 González-Sanchis, M., Murillo, J., Latorre, B., Comín, F., García-Navarro, P., 2012.
818 Transient two-dimensional simulation of real flood events in a Mediterranean
819 floodplain. J.Hydraul.Eng. 1380 (7), 629-641.

820 Goodrich, D.C. 1990. Geometric simplification of a distributed rainfall-runoff model
821 over a range of basin scales, Ph. D. Thesis, University of Arizona, 361 pp.

822 Hall, J.W., Tarantola, S., Bates, P.D., Horritt, M.S., 2005. Distributed Sensitivity
823 Analysis of Flood Inundation Model Calibration. J. Hydraul. Eng.
824 doi:10.1061/(ASCE)0733-9429(2005)131:2(117)

825 Horritt, M., Bates, P., 2001. Predicting floodplain inundation: raster-based modelling
826 versus the finite-element approach. Hydrol.Process. 15, 825-842.

827 House, P.K., Baker, V.R., 2001. Paleohydrology of flash floods in small desert
828 watersheds in western Arizona. Water Resour.Res. 37 (6), 1825-1839.
829 doi:10.1029/2000WR900408.

830 Lacasta, A., Morales-Hernández, M., Murillo, J., García-Navarro, P., 2014. An
831 optimized GPU implementation of a 2D free surface simulation model on unstructured
832 meshes. Adv.Eng.Software. 78, 1-15.

833 Lara, A., Saurí, D., Ribas, A., Pavón, D., 2010. Social perceptions of floods and flood
834 management in a Mediterranean area(Costa Brava, Spain). Natural Hazards and Earth
835 System Sciences. 10, 2081-2091.doi:10.5194/nhess-10-2081-2010.

836 Llasat, M.C., Marcos, R., Llasat-Botija, M., Gilabert, J., Turco, M., Quintana-Seguí, P.,
837 2014. Flash flood evolution in North-Western Mediterranean. Atmos. Res. 149, 230–
838 243. doi:10.1016/j.atmosres.2014.05.024

839 Marchi, L., Borga, M., Preciso, E., Gaume, E., 2010. Characterisation of selected
840 extreme flash floods in Europe and implications for flood risk management. Journal of
841 Hydrology. 394, 118-133. doi:10.1016/j.jhydrol.2010.07.017.

Martin-Vide, J., 2004. Spatial distribution of a daily precipitation concentration index in peninsular Spain. Int.J.Climatol. 24, 959-971.

McGaughey, R., 2009. FUSION/LDV: Software for LIDAR data analysis and visualization. US Department of Agriculture, Forest Service, Pacific Northwest Research Station: Seattle, WA, USA. 123.

Morales-Hernández, M., García-Navarro, P., Burguete, J., Brufau, P., 2013. A conservative strategy to couple 1D and 2D models for shallow water flow simulation. Comput.Fluids. 81, 26-44.

Murillo, J., García-Navarro, P., 2010. Weak solutions for partial differential equations with source terms: Application to the shallow water equations. Journal of Computational Physics. 229, 4327-4368.

Nanson, G.C., Tooth, S., Knighton, A.D., 2002. A global perspective on dryland rivers: perceptions, misconceptions, and distinctions, in: Bull, L.J., Kirkby, M.J. (Eds.), Dryland Rivers: Hydrology and Geomorphology of Semiarid Channels. John Wiley and Sons, New York, pp. 17–54.

Nash, J., Sutcliffe, J.V., 1970. River flow forecasting through conceptual models part I—A discussion of principles. Journal of hydrology. 10, 282-290. doi:10.1016/0022-1694(70)90255-6.

National Research Council. Committee on Alluvial Fan Flooding (NRC), 1996. Alluvial fan flooding, Washington, D.C., National Academy Press.

862 Nikolopoulos, E.I., Anagnostou, E.N., Borga, M., Vivoni, E.R., Papadopoulos, A.,
863 2011. Sensitivity of a mountain basin flash flood to initial wetness condition and rainfall
864 variability. J. Hydrol. 402, 165–178. doi:10.1016/j.jhydrol.2010.12.020

865 Norbiato, D., Borga, M., Degli Esposti, S., Gaume, E., Anquetin, S., 2008. Flash flood
866 warning based on rainfall thresholds and soil moisture conditions: An assessment for
867 gauged and ungauged basins. Journal of Hydrology. 362, 274-290.
868 doi:10.1016/j.jhydrol.2008.08.023.

869 Pappenberger, F., Beven, K., Horritt, M., Blazkova, S., 2005. Uncertainty in the
870 calibration of effective roughness parameters in HEC-RAS using inundation and
871 downstream level observations. J. Hydrol. 302, 46–69.
872 doi:10.1016/j.jhydrol.2004.06.036

873 Pappenberger, F., Frodsham, K., Beven, K., Romanowicz, R., Matgen, P., 2007. Fuzzy
874 set approach to calibrating distributed flood inundation models using remote sensing
875 observations. Hydrol. Earth Syst. Sci. doi:10.5194/hess-11-739-2007

876 Pastor, F., Gómez, I., Estrela, M., 2010. Numerical study of the October 2007 flash
877 flood in the Valencia region (Eastern Spain): the role of orography. Nat Hazards Earth
878 Syst Sci. 10, 1331-1345. doi:10.5194/nhess-10-1331-2010.

879 PCRG 2009. Simulación de la riada del Girona de 2007, Plataforma Ciutadana Girona
880 River https://vimeo.com/5487707.

881 Pilgrim, D. H., Chapman, T. G., Doran, D. G., 1988. Problems of rainfall-runoff
882 modelling in arid and semiarid regions. Hydrological Sciences Journal,33(4), 379-
883 400.doi:10.1080/02626668809491261

884 Rhee, D.S., Woo, H., Kwon, B., Ahn, H.K., 2008. Hydraulic resistance of some selected
885 vegetation in open channel flows. River research and applications. 24 (5), 673-687.

886 Roe, P.L., 1981. Approximate Riemann solvers, parameter vectors, and difference
887 schemes. Journal of computational physics. 43, 357-372.

888 Salazar, S., Francés, F., Komma, J., Blume, T., Francke, T., Bronstert, A., Blöschl, G.,
889 2013. A comparative analysis of the effectiveness of flood management measures based
890 on the concept of" retaining water in the landscape" in different European hydro-
891 climatic regions. Natural Hazards and Earth System Science. 12, 3287-3306.
892 doi:10.5194/nhess-12-3287-2012.

893 Santangelo, N., Daunis-i-Estadella, J., Di Crescenzo, G., Di Donato, V., Faillace, P.,
894 Martín-Fernández, J., ,2012. Topographic predictors of susceptibility to alluvial fan
895 flooding, Southern Apennines. Earth Surf.Process.Landforms. 37 (8), 803-817.

896 Saxton, K.E., Rawls, W.J., 2006. Soil Water Characteristic Estimates by Texture and
897 Organic Matter for Hydrologic Solutions. Soil Sci. Soc. Am. J. 70, 1569–1578.
898 doi:10.2136/sssaj2005.0117

899 Schumann, G., Bates, P.D., Horritt, M.S., Matgen, P., Pappenberger, F., 2009. Progress
900 in integration of remote sensing-derived flood extent and stage data and hydraulic
901 models. Rev. Geophys. 47. doi:10.1029/2008RG000274

902 Segura Beltrán, F., 1990. Las ramblas valencianas: algunos aspectos de hidrología,
903 geomorfología y sedimentología. Universitat de València, València, p. 229.

904 Segura Beltrán, F., 2003. Model d'inundacions en ventalls al.luvials: el cas de les planes
905 costaneres valencianes. Cuadernos de Geografía, 73-74, 207-232.

906 Segura Beltrán, F., 2009. Geomorfología, inundaciones y alteración antrópica del
907 espacio inundable: el caso del riu Girona (Alacant, octubre de 2007). Boletín de la
908 Asociación de Geógrafos Españoles., 83-103.

909 Tayefi, V., Lane, S., Hardy, R., Yu, D., 2007. A comparison of one-and
910 two-dimensional approaches to modelling flood inundation over complex upland
911 floodplains. Hydrol.Process. 21, 3190-3202.

912 Toro, E.F. 2001. Shock-Capturing Methods for Free-Surface Shallow Flows. Wiley,
913 New York, p. 109.

914 Vannier, O., Braud, I., Anquetin, S., 2013. Regional estimation of catchment-scale soil
915 properties by means of streamflow recession analysis for use in distributed hydrological
916 models. Hydrol. Process. n/a. doi:10.1002/hyp.10101

917 Vegas, R.; Pedraza, J; Zazo, C; Goy, J. L.; Cabañas, J.; Uralde, M. A. (1975): Mapa
918 Geológico de Gandia. Hoja 796. Memoria y cartografía. IGME, Madrid.

919 Vélez, J.J., Francés, F., 2005. Automatic calibration of initial state variables for flood
920 forecasting using a distributed model. Int. Conf. Innov. Adv. Implement. flood Forecast.
921 Technol. 17 to 19 Oct. 2005, Tromsø, Norw.

922 Vélez, J.J., Puricelli, M., López Unzu, F., Francés, F., 2009. Parameter extrapolation to
923 ungauged basins with a hydrological distributed model in a regional framework.
924 Hydrology and earth system sciences. 13, 229-246. doi:10.5194/hess-13-229-2009

925 Yatheendradas, S., Wagener, T., Gupta, H., Unkrich, C., Goodrich, D., Schaffner, M., et
926 al., 2008. Understanding uncertainty in distributed flash flood forecasting for semiarid
927 regions. Water Resour.Res. 44 (5). doi:10.1029/2007WR005940.

***Highlights (for review)**

We simulated the Girona River flash flood using hydrologic and hydraulic models

Models results were validated with post-flood surveys

The connection between geomorphologic structure and flooded area was analyzed

We identified flood activation thresholds in different geomorphic elements

Figure captions

Figure 1. Sketch of the Girona River basin. Location of the model area is indicated through the red polygon beside the coastline.

Figure 2. Location of the rainfall observatories used for event reconstruction and hydrologic modeling.

Figure 3. Rainfall intensity at Isbert and Gallinera observatories (a), and Guadalest reservoir (b) during the October 2007 event.

Figure 4. Post-flood surveys information and final observed flooded area used for hydraulic model validation.

Figure 5. Observed and simulate hydrographs at the Guadalest Reservoir for all the events used for model calibration and validation.

Figure 6. Simulate hydrographs of the Girona River. The red solid line represents the simulated hydrograph obtained calibrating the initial soil storage based on post-flood information. The grey-shaded area lines represents the simulated hydrograph range obtained using initial soil moisture spanning from 35% to 60% of soil saturation capacity.

Figure 7. Flooded area and flood depth obtained with the final simulation of the hydraulic model, under flow conditions of 515 $m^3 s^{-1}$.

Figure 8. Geomorphologic map of the model area.

Figure 9. Model simulations with different flow conditions a) 400 $m^3 s^{-1}$; b) 515 $m^3 s^{-1}$; c) 900 $m^3 s^{-1}$. Geomorphologic mapping is represented to show the activation of the different alluvial fans, palaeochannels and depressions under different flow conditions.

Only for black and white edition:

Figure 1. Sketch of the Girona River basin. Location of the model area is indicated through the polygon beside the coastline.

Figure 1

Click here to download high resolution image

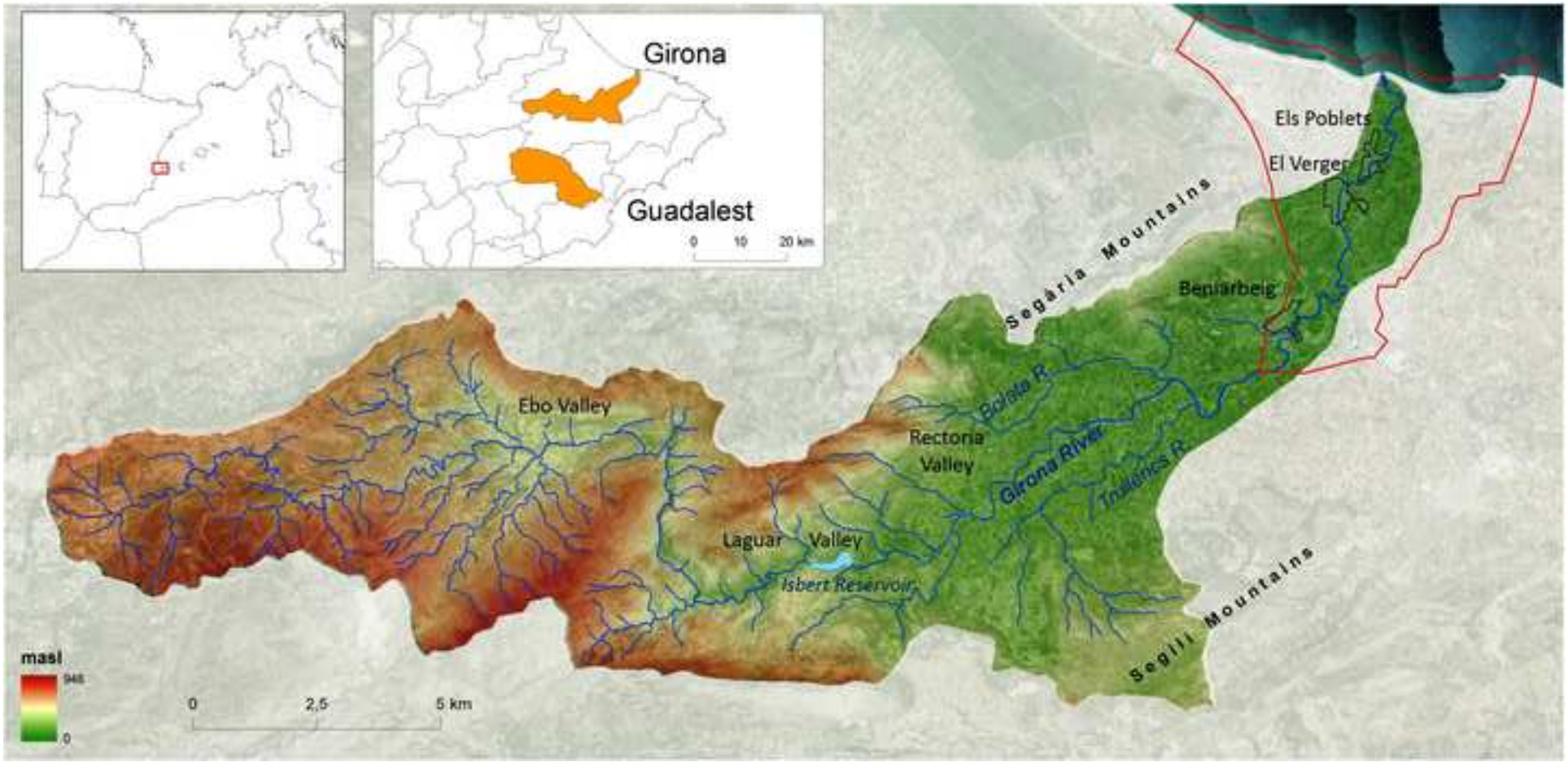

Figure 2

Click here to download high resolution image

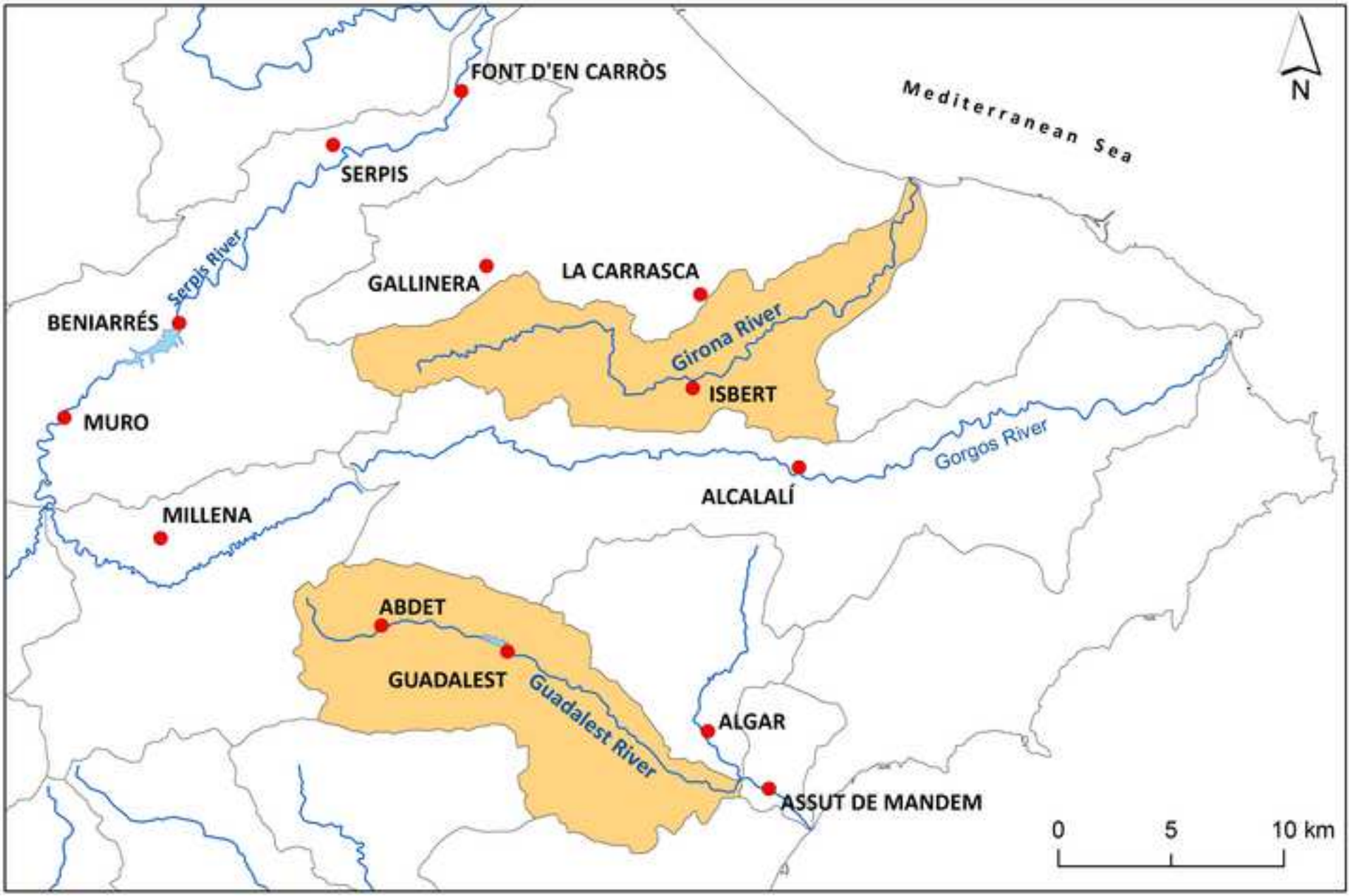

Figure 3ab

Click here to download high resolution image

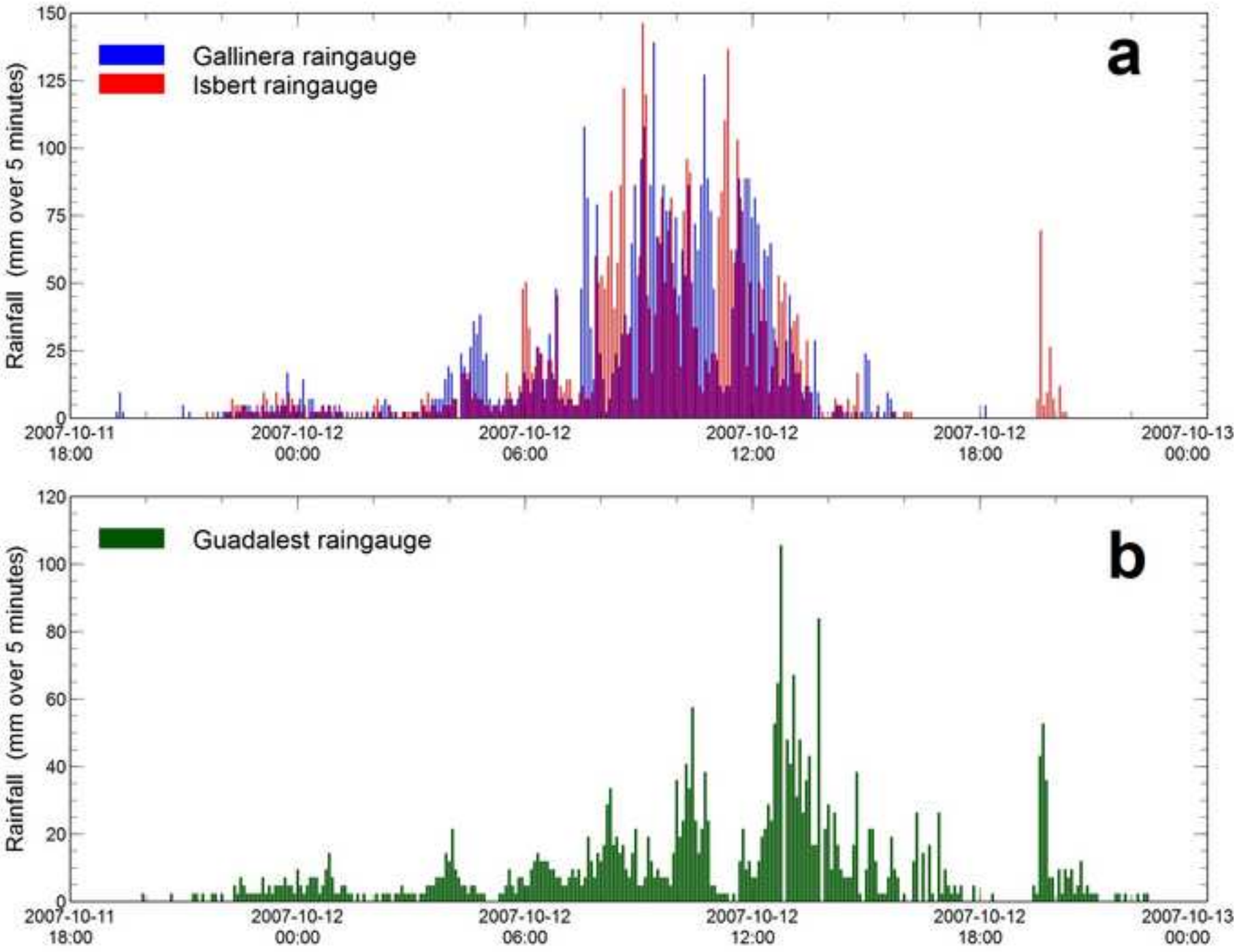

Figure 4

Click here to download high resolution image

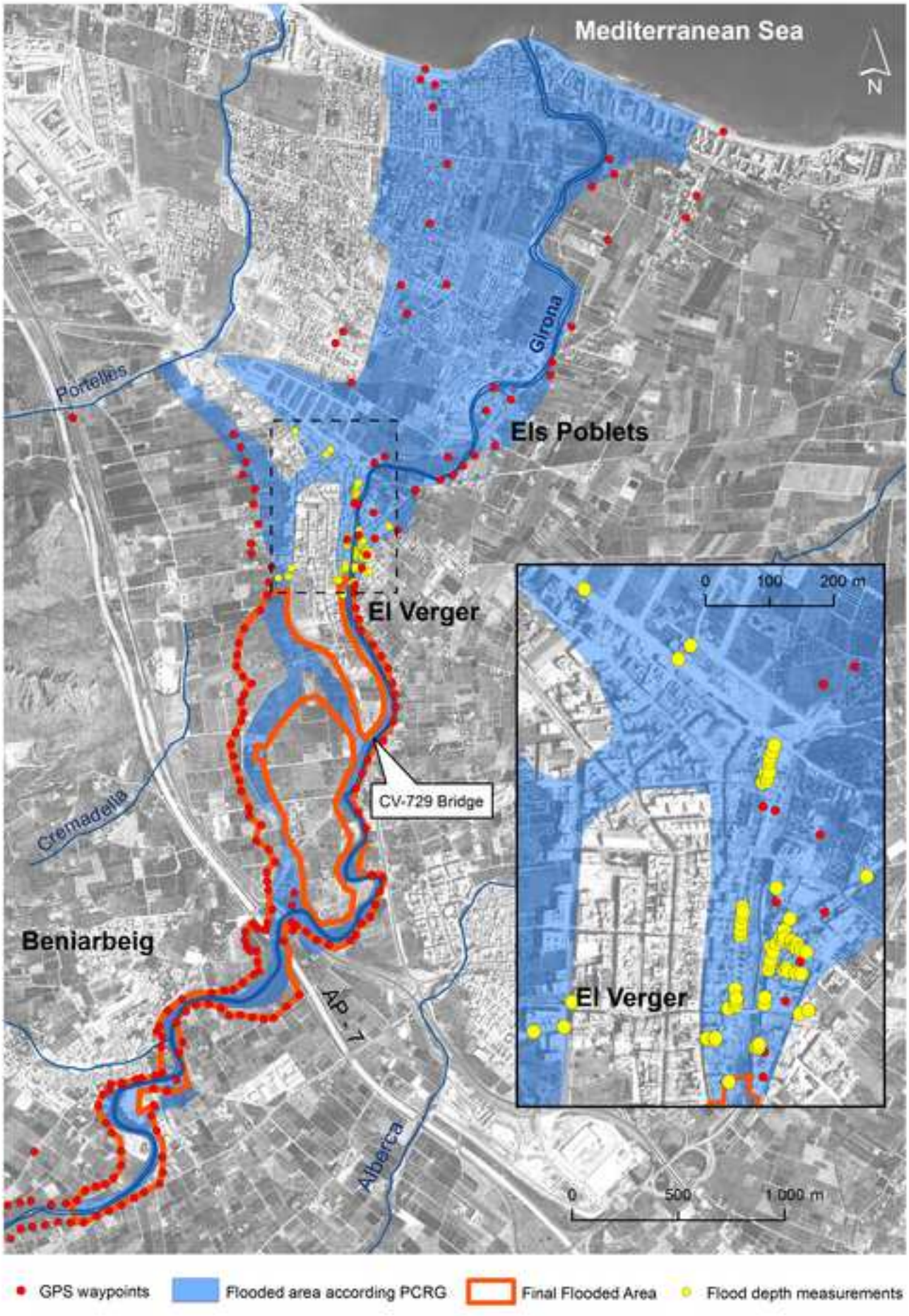

Figure 5

Click here to download high resolution image

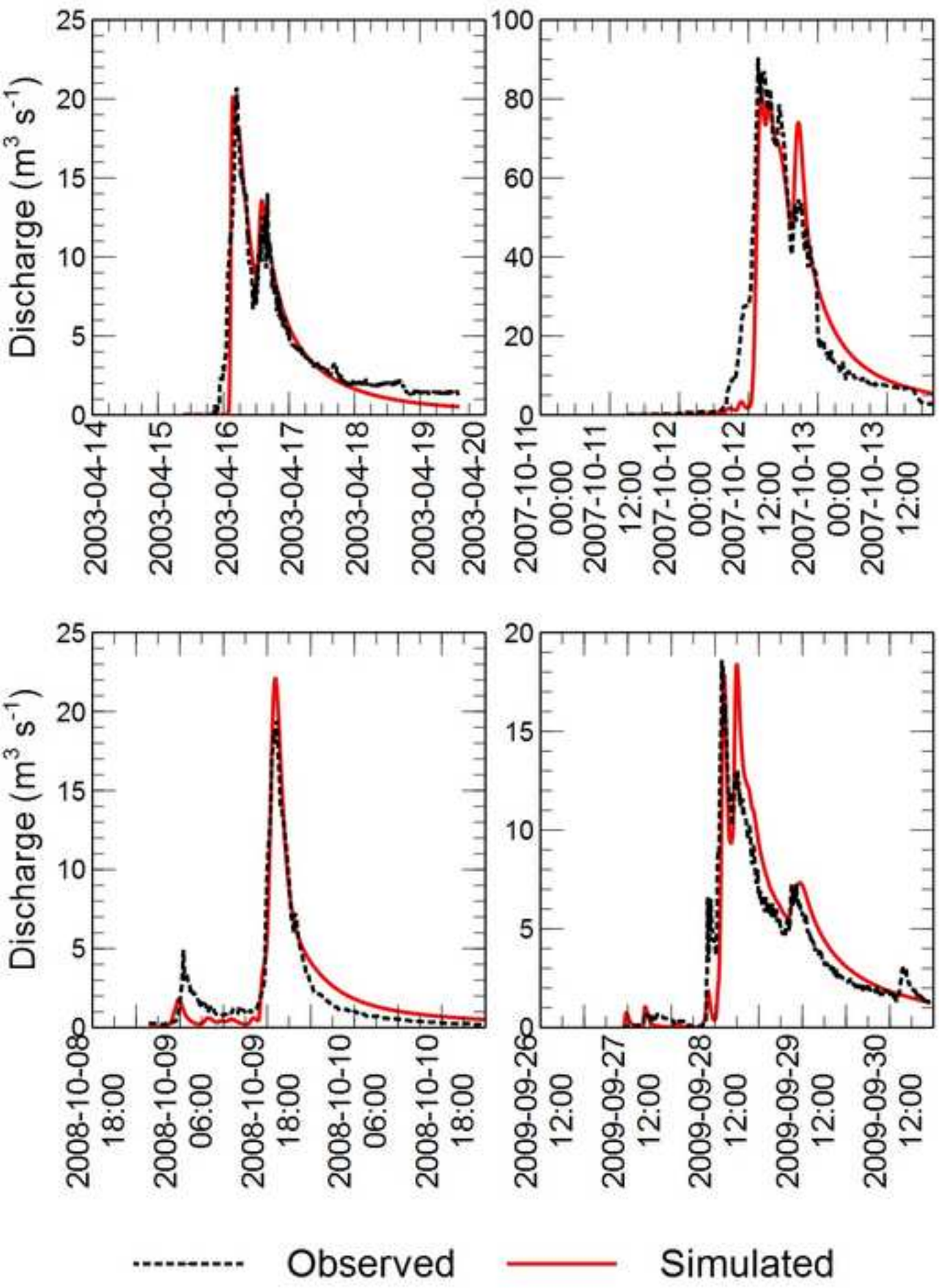

Figure 6

Click here to download high resolution image

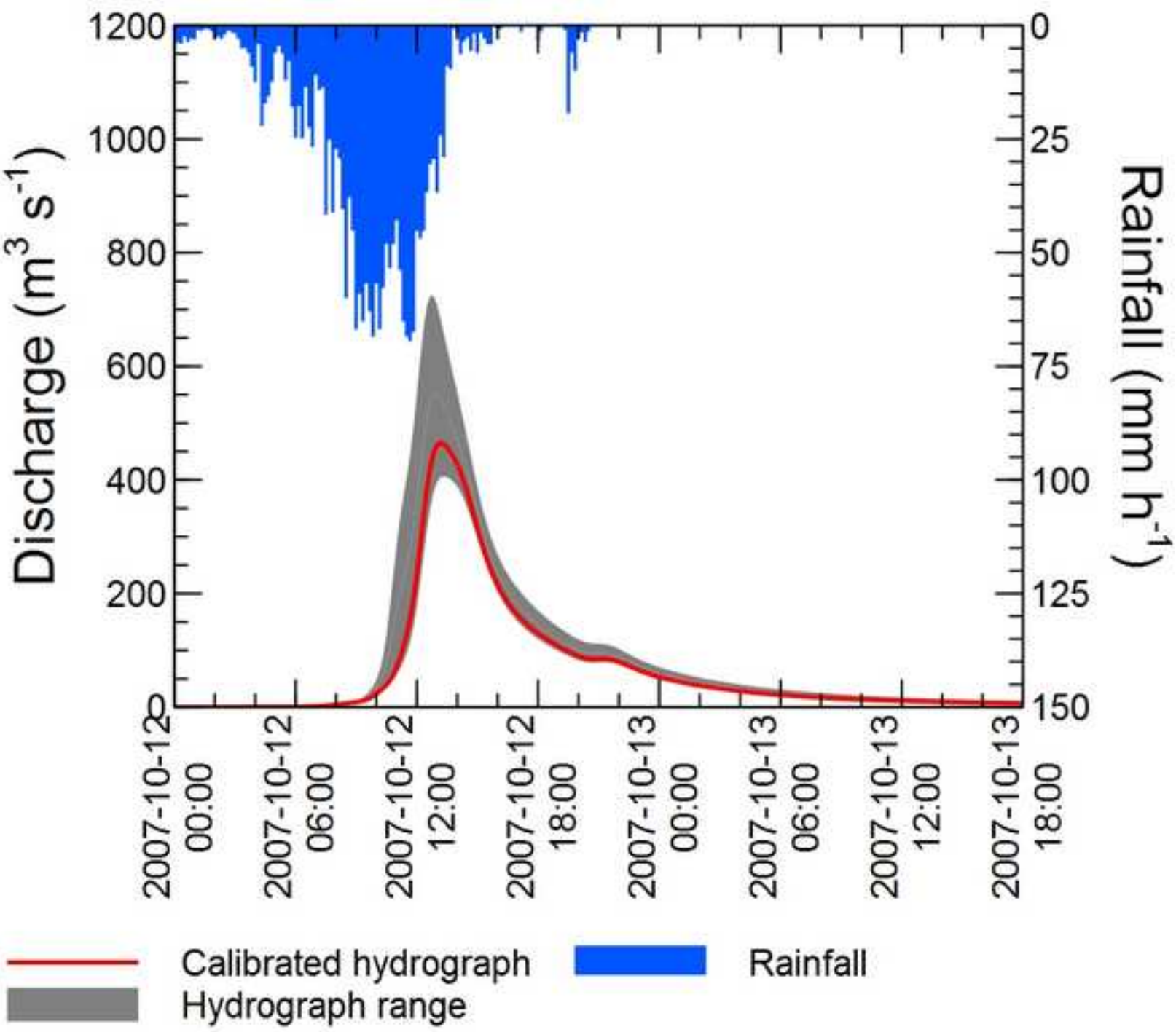

Figure 7

Click here to download high resolution image

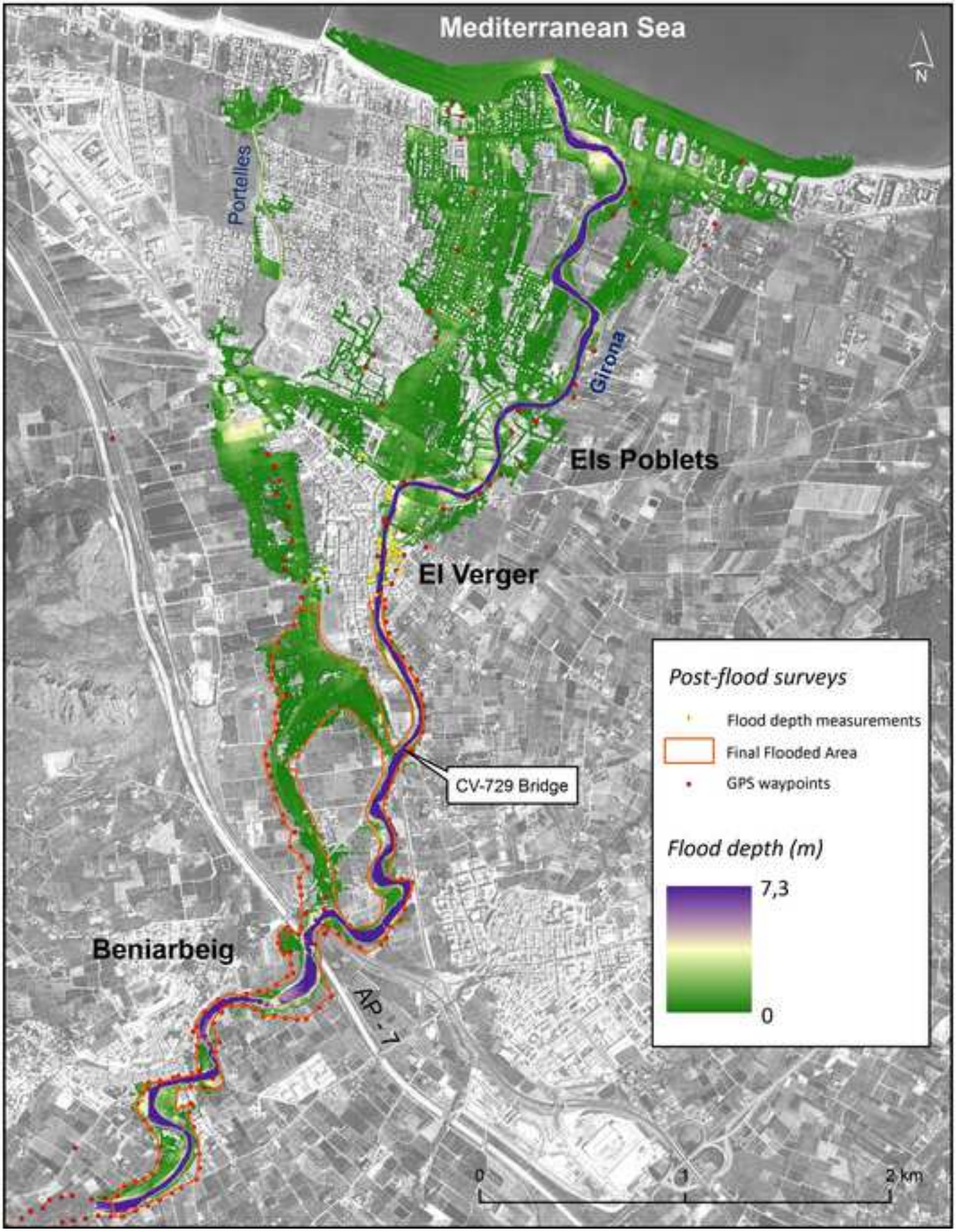

Figure 8

Click here to download high resolution image

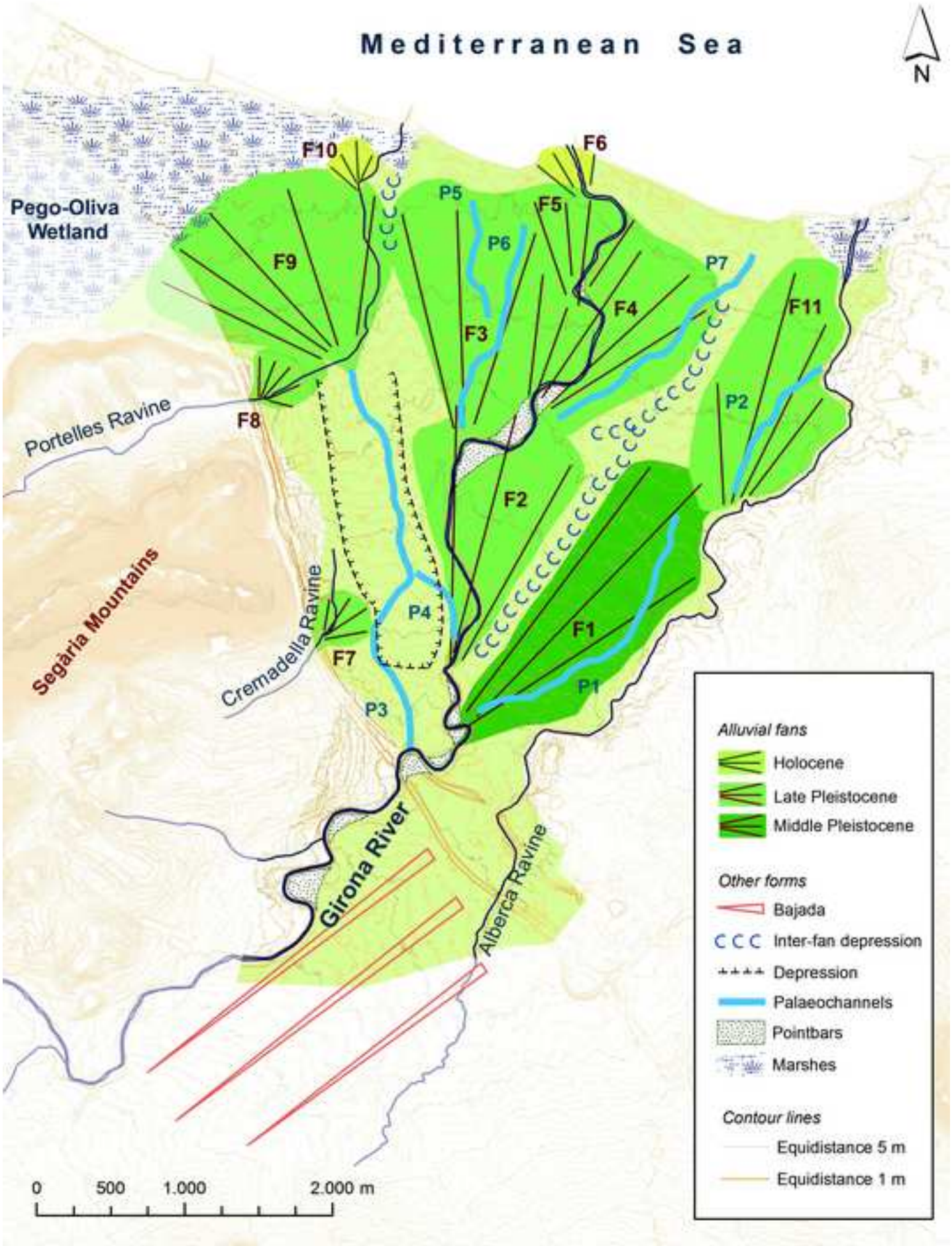

Figure 9

Click here to download high resolution image

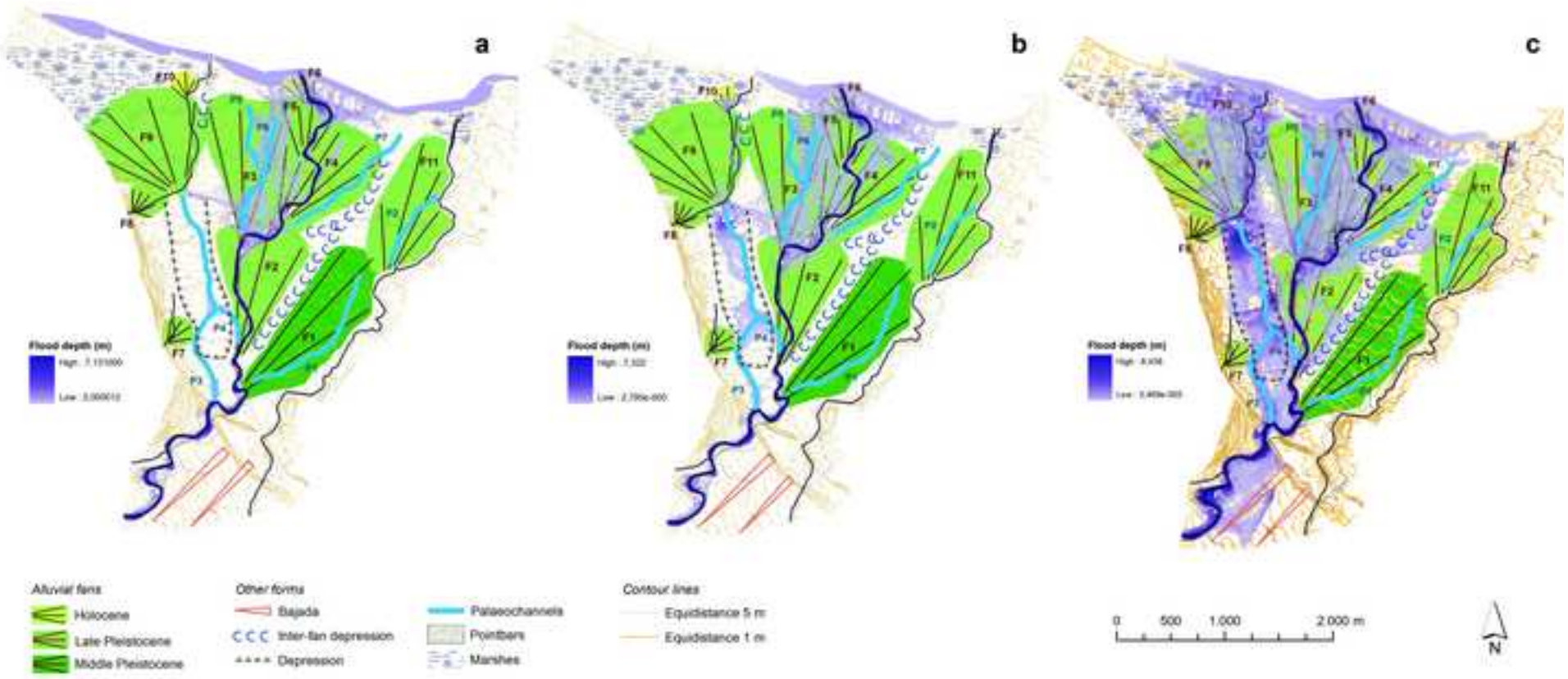

Figure 1 for black and white

Click here to download high resolution image

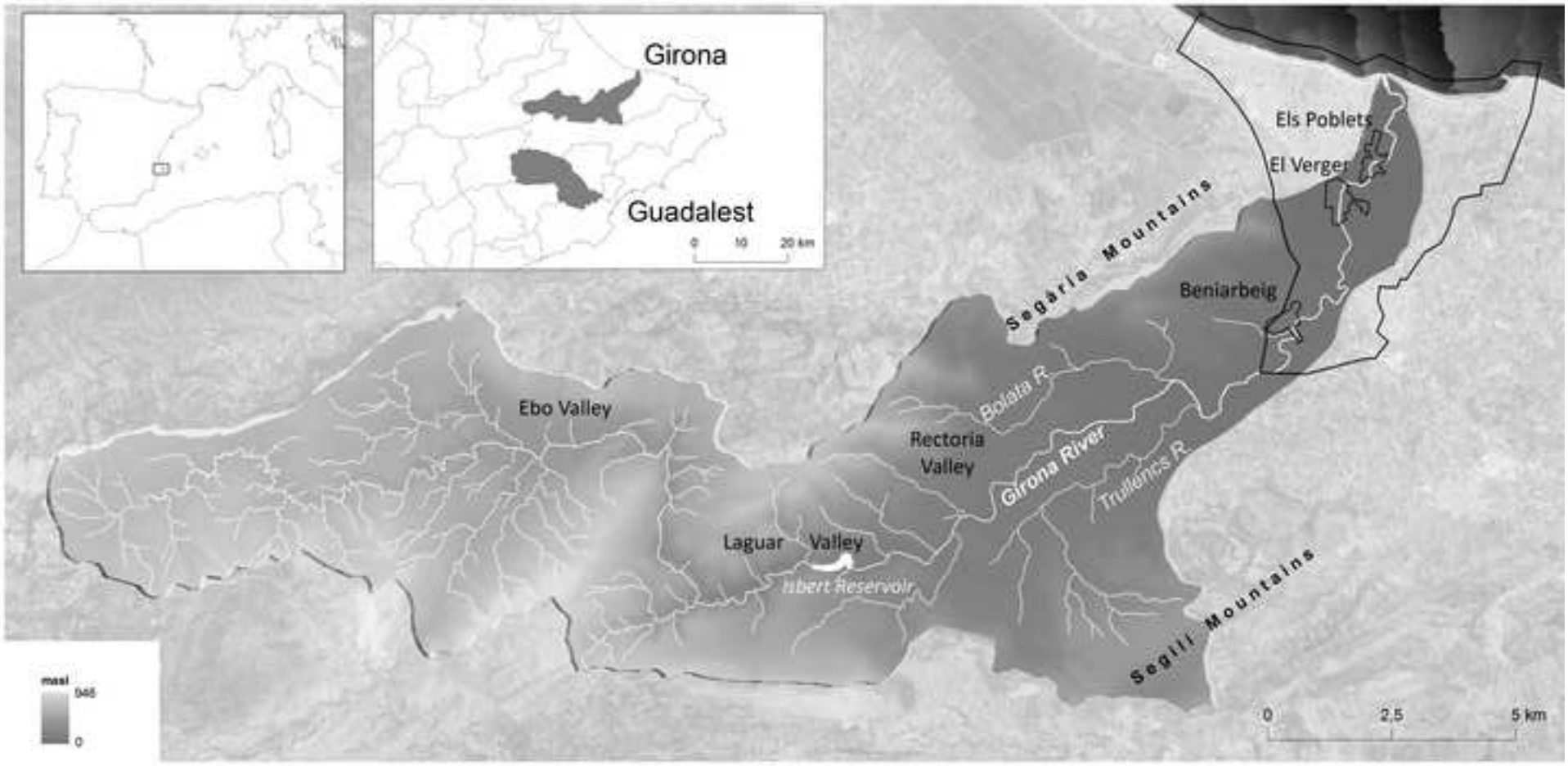

Figure 3 for black and white

Click here to download high resolution image

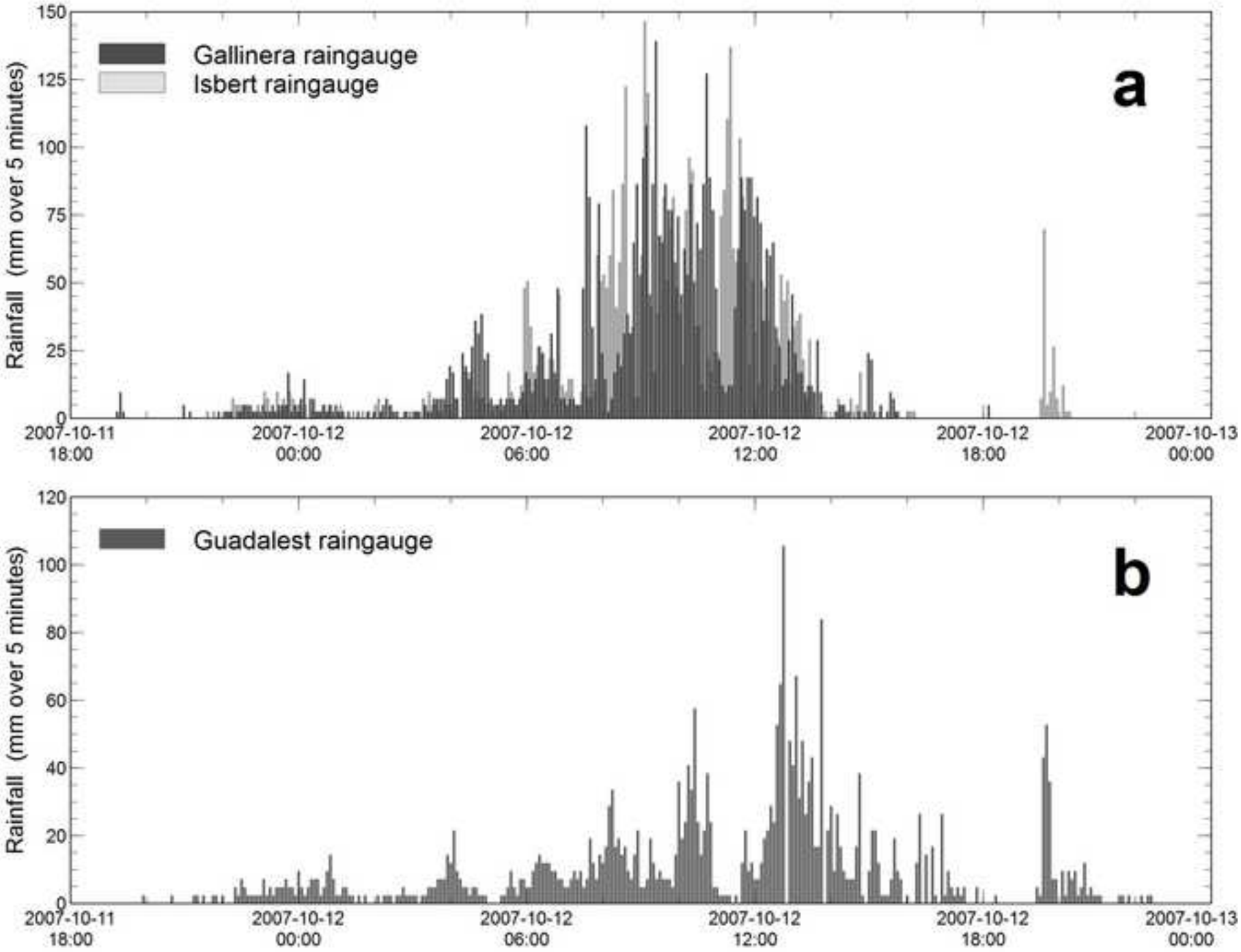

Figure 4 for black and white publishing

Click here to download high resolution image

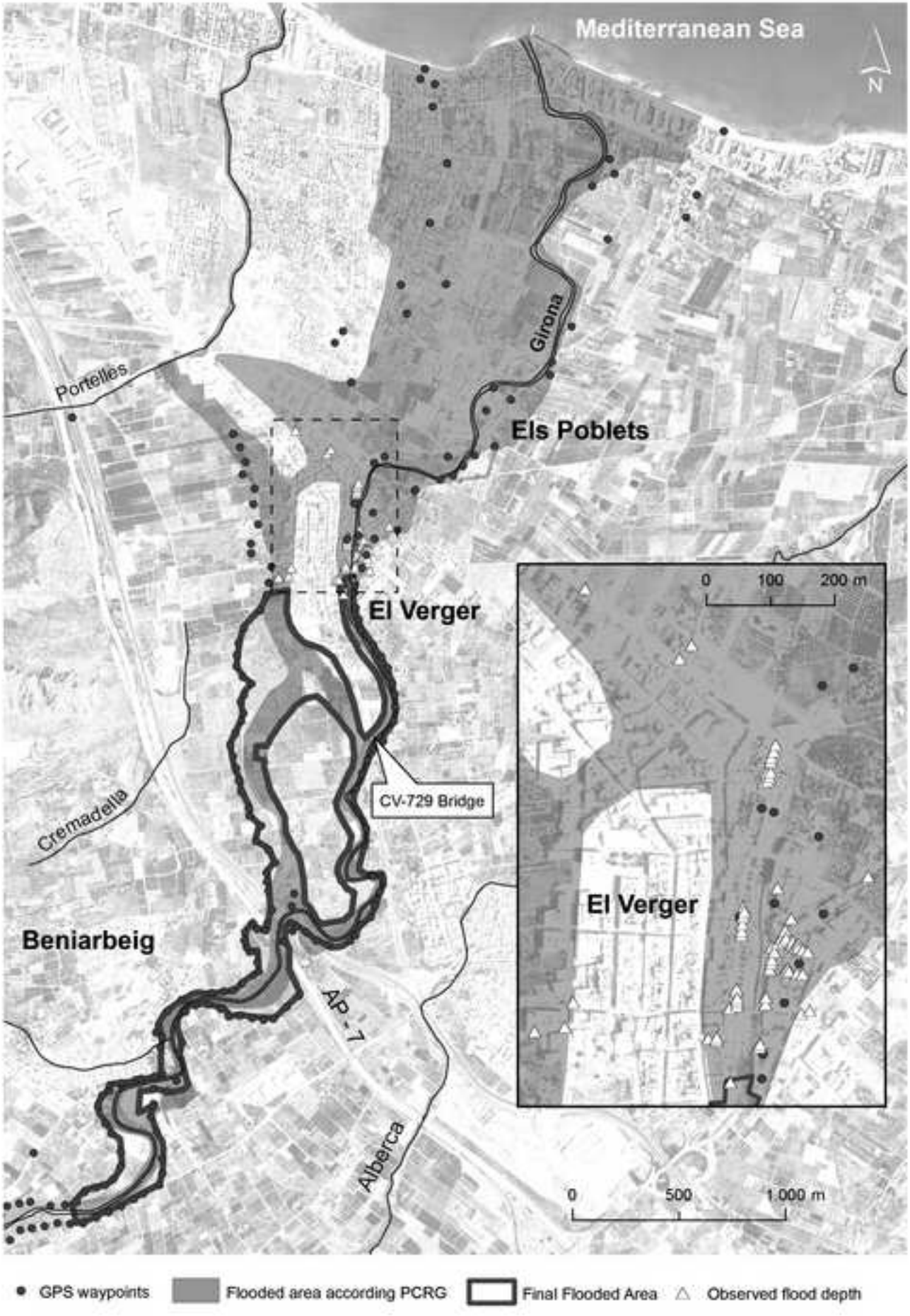

Figure 7 for black and white
Click here to download high resolution image

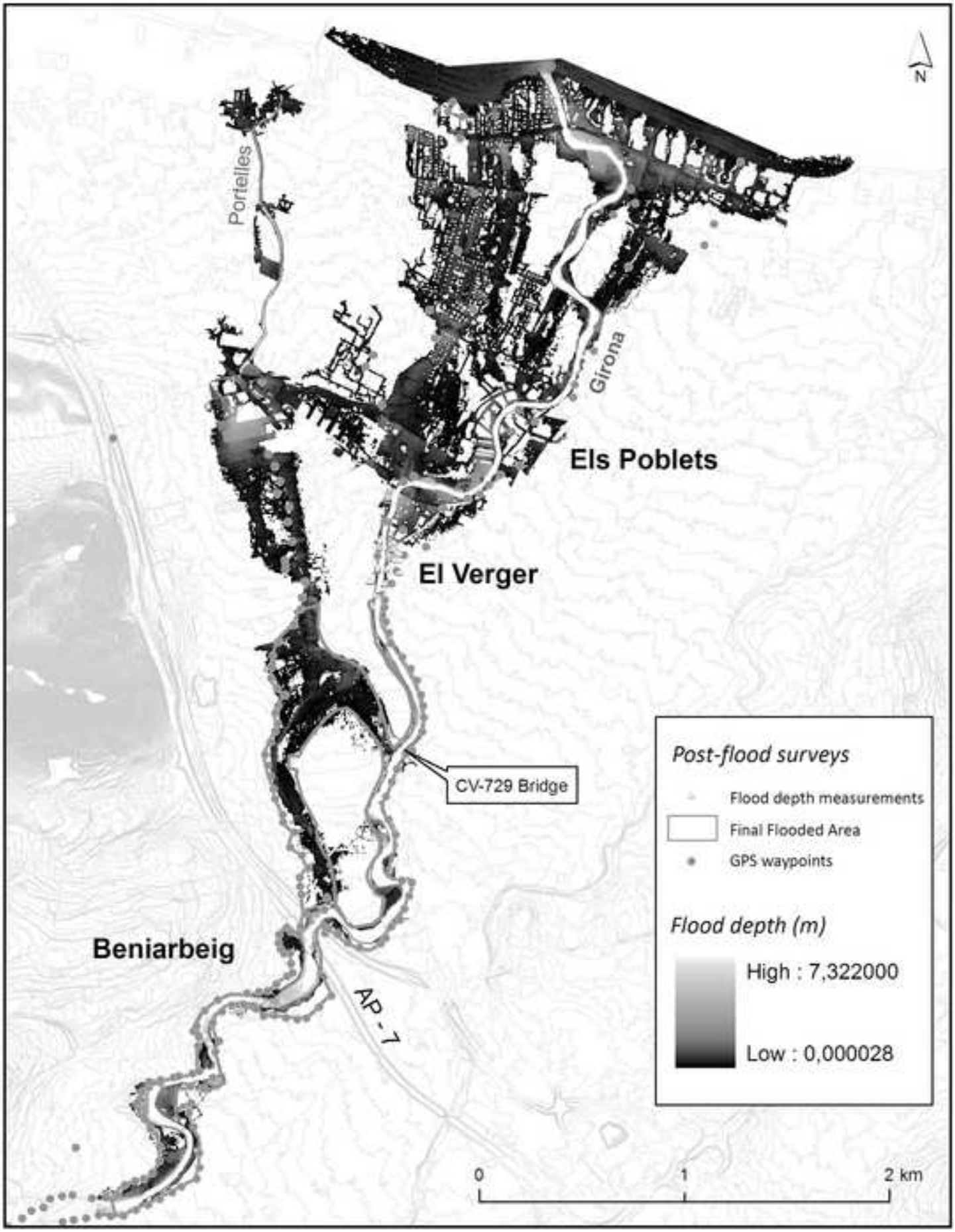

Figure 8 for black and white

Click here to download high resolution image

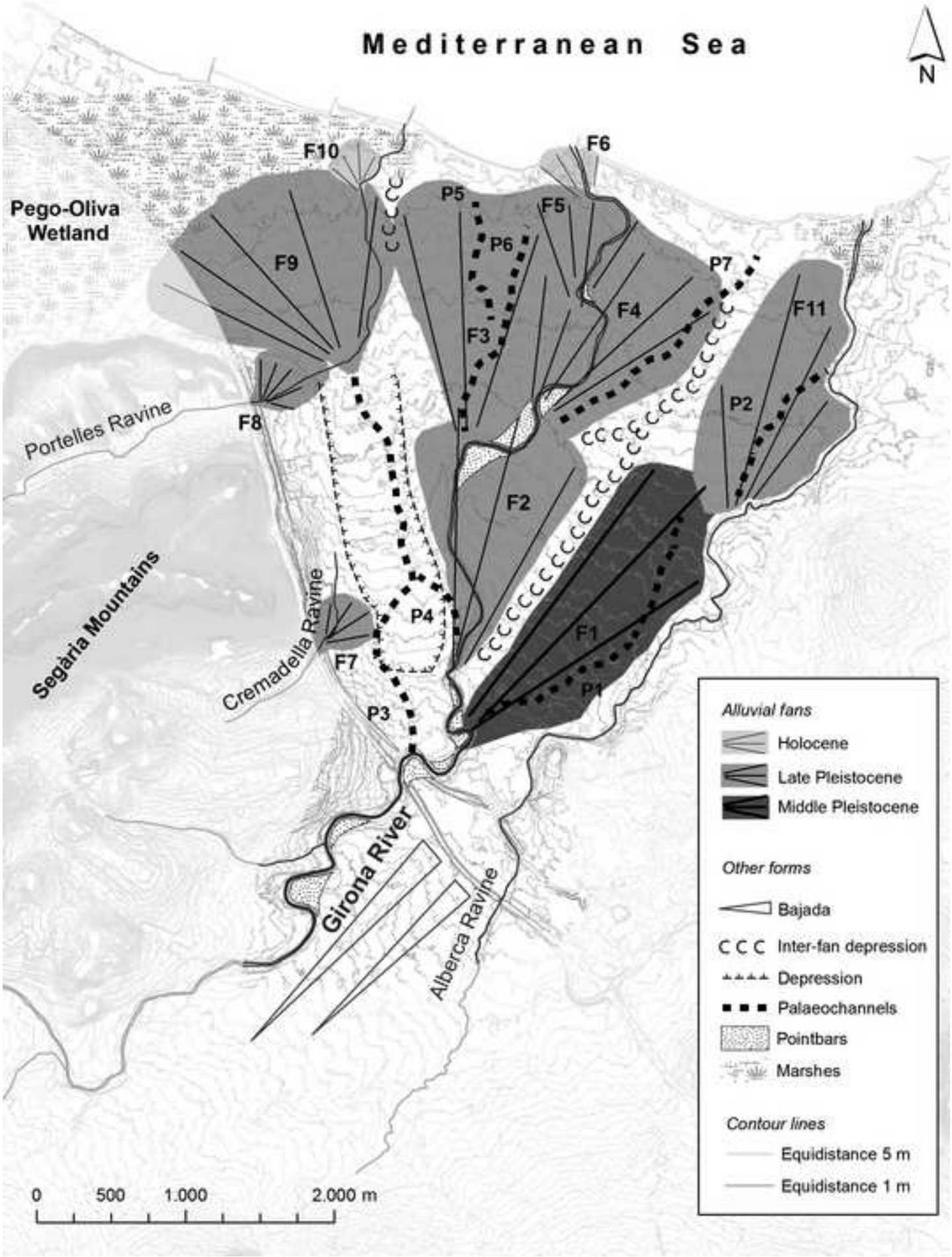

Figure 9 for black and white

Click here to download high resolution image